UNIVERSITY OF COPENHAGEN

MSc in Physics

Sterile Neutrinos in The Early Universe

Numerical Simulation of 2 Active and 1 Sterile Flavour Neutrino model in the Early Universe

Rohan Kumar

Supervised by Irene Tamborra

Nov 2020

Rohan Kumar
Sterile Neutrinos in The Early Universe
MSc in Physics, Nov 2020
Supervisor: Irene Tamborra

University of Copenhagen
Niels Bohr Institute
Masters Degree in Physics
Blegdamsvej 17
2200 Copenhagen

Preface

This thesis presents the research conducted as a part of my Master of Science degree in Physics at the University of Copenhagen. It aims to study the sterile neutrinos in a 2 active and 1 sterile flavour configuration (2+1 model) in early universe plasma in 60 MeV to 1 MeV Temperature range. Numerical simulations of 1+1 model and 2+1 model have been carried out in a parameter range of interest. A comparison between the average and multi-momentum models has been presented to better illustrate the impact of active-active oscillation in case of 2+1 scenario to the best of my abilities.

Acknowledgements

First and Foremost, I want to extend my greatly felt appreciation and gratitude to my thesis supervisor Irene Tamborra, for her constant support even when things were not going as planned. She also helped me in gaining knowledge beyond my thesis by organizing weekly group meeting, where group members could exchange their ideas. This created an overwhelmingly great research environment that I could have imagined.

I would also like to thanks my Astro-Neutrino group members, especially Shashank Shalgar for lending his help when I required it during the beginning of my thesis and Anna Suliga for helping with the Super-computer tasks.

I would take the opportunity to thanks and appreciate the constant support by my parents who were always there for me and supported me in pursuing my love for Physics. Their love and motivation for me made my master degree a pleasant endeavour.

Abstract

There has been significant interest in the neutrino physics over anomalies in the LSND, MiniBoone detector and reactor anomalies, this leads to a speculative interest in the possibility of a sterile neutrino without weak-interactions. The existence of such a neutrino specie could also explain the deviation of effective degrees of freedom N_{eff} in the cosmological perspective. Thesis focuses on 2+1 flavour model with dynamic Lepton Asymmetries, and aims to puts constraints on mixing parameters between active-sterile parameters based on final N_{eff} values that are within the observation range allowed by the Planck 2018 results.

Contents

1 Introduction **1**

2 Neutrinos **3**
2.1 The Standard Model Neutrinos 3
2.2 Fourth Generation Neutrinos 4
2.3 Neutrino Anomalies 4
2.4 Cosmological Bounds on Fourth Neutrino 4
2.5 Sterile Neutrinos 5
2.6 Lepton Asymmetry 5

3 Neutrino Oscillations **7**
3.1 Neutrino Oscillations 7
3.2 Density Matrix Formalism 7
3.3 Time Evolution of Density Matrix 9

4 Dense Media Effects **13**
4.1 Primordial Dense Media 13
4.2 Coherent Forward Scattering 14
4.3 Active-Sterile Potentials 14
4.4 Active-Active Potentials 16
4.5 Matter-AntiMatter Potentials 16
4.6 Damping Effects 16
4.7 Repopulation effects 17

5 2 Active and 1 Sterile Flavour Model **19**
5.1 2+1 flavour mixing 19
5.2 Quantum Kinetic Equation for 2+1 flavour model 21
5.2.1 Damping and Repopulation Terms 22
5.3 Evolution of Lepton Asymmetry 24
5.3.1 Evolution equations for Anti-Neutrinos 25
5.4 Evolution with Temperature 25

5.4.1 Effective Degrees of Freedom, N_{eff} 26
5.5 Commutator Values by Expanding Einstein Summations 27

6 Numerical Simulations and Results **29**
6.1 Details of Numerical Computation 29
6.2 Numerical Evolution of Density Matrix 1+1 model 29
6.2.1 1+1 Flavour model with Zero Asymmetry 30
6.2.2 1+1 Flavour model with Non Zero Asymmetry 33
6.2.3 1+1 Model Evolution for Positive Δm^2 33
6.3 Numerical Evolution of 2+1 model 36
6.4 Dynamics of N_{eff} 36
6.5 Dynamics of Lepton Asymmetries 37
6.5.1 2+1 Flavour Average Momentum Model with zero asymmetry 38
6.5.2 2+1 Average Momentum Model with Non Zero Asymmetry 41
6.5.3 2+1 Multi-momentum Model with Zero Asymmetries . . 44
6.5.4 2+1 Multi-momentum Model with Non-Zero Asymmetries 47

7 Discussion **53**
7.1 Summary of findings 53
7.1.1 Average momentum 2+1 model 53
7.1.2 Multi-momentum 2+1 model 54

8 Perspectives **55**

9 Bibliography **57**

1 Introduction

The Early Universe was a high-energy playground for Particle Physics with plenty of interesting phenomena, such as electron-positron annihilation to produce Cosmic Microwave Background (CMB), structure formation leading to deviations in CMB, Big Bang Nucleosynthesis leading to production of light elements, Spontaneous Symmetry Breaking leading to boson and fermion masses. A lot of these phenomenon can be measured and tracked with high details. Thus it can be seen that Particle Physics plays a crucial role in development of our Universe. The Standard Model (SM) of Particle Physics provides us with a good understanding of such phenomena.

There are also some early universe phenomena that are being studied in various scenarios, but the search for a consistent model is still on. Beyond SM particle physics, such as looking for a fourth generation of fermions has been empty handed so far. This makes observations of effective number of neutrinos being allowed to be slightly more than 3, an interesting beyond SM physics question to be answered.

One other mystery is the absence of anti-matter from the Universe. The baryonic asymmetry is measured to be around 10^{-10} by a number of experiments. The lepton asymmetry, however, has not been measured. This can be reasoned by the weakly interacting nature of uncharged neutrinos which makes this endeavour even more troublesome.

This thesis focuses a non-SM Sterile Neutrino that interacts only via gravitational interaction and Neutrino Oscillations. Developing a model for such a neutrino for a 2+1 scenario is the goal of this thesis.

Neutrino flavor conversions are important in the Early Universe and they may affect observable cosmological quantities like effective degrees of freedom and lepton asymmetry. The thesis focuses on understanding the interplay between active and sterile neutrino conversions in the hypothesis that extra

sterile neutrino families exist. A Numerical Model of 1 Sterile Neutrino along with 2 Active Flavour species has been studied and estimations of the flavor evolution is derived in the energy ranges 60-1 MeV. A comparison between the 1+1 model and 2+1 model for sterile neutrino has also been carried out.

Neutrinos

2

2.1 The Standard Model Neutrinos

The Standard Model of Particle Physics describes the fundamental elementary particles and the interactions between them, experienced by the exchange of some particles, known as bosons. The fermions are broadly classified over 3 generation of particles ranging from the lightest particles being called the first generation and the heavier ones described as higher generations with increasing order of mass range. The different generation display the same interactions and the only parameter to differentiate them is their range of masses. The neutrinos are also divided among 3 generation of particles with flavours named after their leptonic partners, electron, muon, and tau leptons. However, the ordering of masses for neutrinos is very much debatable, this problem is more colloquially referred to as the mass hierarchy problem.

The ordering of neutrino masses becomes a greatly different topic than for their leptonic counterparts because of their mass eigenstates being different from their flavour eigenstates, and the lightness of neutrinos that gives rise to the phenomenon of neutrino oscillations. This phenomenon not only describes the change in neutrino flavour values as they travel, but it also predicts the presence of MSW resonances for solar electron neutrinos inside the sun, which was later verified [1][2]. For the resonance to occur inside matter for the electron flavour the mass ordering between the first and the second mass states should be normal. The values for $\Delta m^2_{21} = 7.6 \times 10^{-5}$ and the mixing angle was found to be $\theta_{12} = 33.45°$ for the first two mass states. The third mass

eigenstate decides the nomenclature of mass ordering, if $m_1 < m_2 < m_3$ the case is referred to as Normal ordering and the case $m_3 < m_1 < m_2$ is called the Inverted ordering.

2.2 Fourth Generation Neutrinos

Before diving in the theory of oscillation, considering how a fourth generation of fermions would modify the Standard Model is also an important bit to tackle. The additional introduction of a fourth neutrino with standard model weak interactions, as that of the 3 known generations would increase the decay width of the Z Bosons, as observed by [3]. The fits performed in this paper [4] also excluded effective number of neutrino species to $N_{eff} = 3.27 \pm 0.30$, whereas the standard model predicts $N_{eff} = 3.046$ [5], which was excluded at 98% confidence limit.

2.3 Neutrino Anomalies

The LSND (Liquid Scintillator Neutrino Detector) was the first short base-line detector to observe neutrino oscillation in $0.2 - 10\ eV^2$ range. [6]. Later in MiniBooNE experiment excess flux for electron anti-neutrinos was also observed which was in line with the observation of excess oscillation of $\bar{\nu}_\mu \rightarrow \bar{\nu}_e$ at $0.1 - 1.0\ eV^2$ range.[7]. The reactor anomalies from various radio-active decay sources also point to a new non-standard model neutrino with $|\Delta m^2| > 1.5 eV^2$ [8].

2.4 Cosmological Bounds on Fourth Neutrino

The weak decoupling approach before 60 MeV, is the time when the active neutrinos were in thermal contact with the background plasma and radiation via the weak-interactions and as the universe expands, the weak-interaction rate that depends upon the temperature of the plasma drops as universe cools down. The lowering of the interaction rate finally falls below the expansion

rate of the universe around 1 MeV, thereby essentially removing any thermal changes in distribution of Dirac Neutrinos. The number of thermalized neutrino species N_{eff} is essentially locked into place as the universe cools after the decoupling. The current value of N_{eff} from the cosmological data and Planck results [9] is $2.96^{+0.34}_{-0.33}$ and the planck results are also in conflict with inverted hierarchy with $\Sigma m_{\nu_i} < 0.12\ eV$. The N_{eff} from the above results allow for extra neutrino species to exist in a non-fully thermalised manner.

2.5 Sterile Neutrinos

The sterile neutrino is a model for a non-standard model neutrino that does not undergo any interactions except for gravitational interaction and can only be produced or converted to other flavours of neutrino via oscillations. The planck data favours models for sterile neutrino with normal mass ordering more than inverted ordering. The thesis focuses on single Dirac sterile neutrino in a 2+1 model, for mass squared difference scale around $1\ eV^2$. The fully thermalised sterile neutrinos are forbidden by the experimental data so far, thus there the alternative of having non-zero lepton asymmetry, which can suppress production of sterile neutrino before the neutrino decoupling is a better one. The existence of a non-zero lepton asymmetry would allow for a non-fully thermalised version of sterile neutrino to be compatible experimental data from experimental particle physics as well as data derived from cosmology observables.

2.6 Lepton Asymmetry

The matter-antimatter content of the early universe during the weak decoupling era determines the neutron-proton ratio and the light element contents such as Helium, Hydrogen and their isotopes. There are a number of mechanism that can lead to a production of a non-zero lepton number [10]. For the entirety of the thesis we assume the lepton asymmetry stems from the active-sterile neutrino oscillations with the sterile species that going inert after the weak decoupling.

This thesis uses a model of dynamics for lepton asymmetry that would conserve overall lepton number. This means the evolution equation for lepton asymmetry does not involve the terms for damping and repopulation, thus the lepton number is conserved. This also means the lepton asymmetry should be evolved separately from the neutrino-antineutrino system.

3 Neutrino Oscillations

3.1 Neutrino Oscillations

First theorised in 1957, Neutrino Oscillations is a phenomenon that allows travelling neutrinos to change flavour among 3 leptonic values. The phenomenon of flavour oscillation is a result of very small neutrinos masses and their comparatively large momenta, as compared to their more massive leptonic counterparts.

Each Neutrino travels as a superposition of mass eigenstates and the time evolution of different mass eigenstates makes them acquires different phase shifts. This results in the flavour of the superposition to change as they travel. The flavour of neutrino can be measured via weak interactions in a large detectors with scintillators and photo-multiplier tubes.

The mixing between leptons is larger than smaller quark mixing. The experimental results from K2K experiment [11] and KamLAND [12] in 2002 confirmed the mixing parameters of the active neutrino sector.

3.2 Density Matrix Formalism

The problem of neutrino oscillations is a quantum many body problem, it requires tracking coherence and phases between different eigenstates. To solve the problem in a simpler fashion, the density matrix formalism is used from this point forward. First, the relation between the mass eigenstates and flavour

eigenstates is to be described. We start with defining the time evolution of mass and flavour eigenstates.

The evolution for mass and flavour states are driven by the hamiltonians H_m and H_f in respective eigenstates.

$$|\psi_m(t)\rangle = e^{-iH_m t} |\psi_m(0)\rangle \tag{3.1}$$

$$|\psi_f(t)\rangle = e^{-iH_f t} |\psi_f(0)\rangle \tag{3.2}$$

Now using 3.2 we can define the flavour density matrix ρ as

$$\rho(0) = |\psi_f(0)\rangle \langle\psi_f(0)| \tag{3.3}$$

where H_m is dependent on kinetic energy as follows

$$H_m = \frac{1}{2E} \begin{bmatrix} m_1^2 & 0 \\ 0 & m_2^2 \end{bmatrix} \tag{3.4}$$

The relation between the two hamiltonian is governed by the mixing matrix U, for simplicity lets take the case for 2 flavour evolution. For mixing angle θ the mixing matrix can be written as

$$U = \begin{bmatrix} cos(\theta) & sin(\theta) \\ -sin(\theta) & cos(\theta) \end{bmatrix} \tag{3.5}$$

This allows for the vacuum flavour hamiltonian H_f to be defined as following

$$H_f = U H_m U^\dagger \tag{3.6}$$

$$H_f = \begin{bmatrix} c^2 m_1^2 + s^2 m_2^2 & cs(m_2^2 - m_1^2) \\ cs(m_2^2 - m_1^2) & s^2 m_1^2 + c^2 m_2^2 \end{bmatrix} \tag{3.7}$$

where $c = cos(\theta)$ & $s = sin(\theta)$

The probabilities for flavour appearance and disappearance can be calculated with $|\langle\psi_f(t)|\psi_f(0)\rangle|^2$. The probability of appearance of a muon neutrino in a electron neutrino beam is given by

$$P_{\nu_e \to \nu_\mu} = sin^2(2\theta) sin^2(\tfrac{\Delta m^2 t}{4E}) \tag{3.8}$$

here $\Delta m^2 = m_2^2 - m_1^2$. The probability above is also known as disappearance probability for ν_e . Similarly by conservation of total probability for 2 flavour case, the survival probability for ν_e i.e. $P_{\nu_e \to \nu_e}$ is given by

$$P_{\nu_e \to \nu_e} = 1 - sin^2(2\theta) sin^2(\tfrac{\Delta m^2 t}{4E}) \tag{3.9}$$

Next, we define the density matrix ρ for the flavour eigenstates of neutrinos in terms of polarization vectors.

$$\rho = \frac{1}{2}(P_0 + \vec{P} \cdot \vec{\sigma}) \tag{3.10}$$

where $\vec{\sigma}$ are the pauli matrices. The above equation can be written in matrix form.

$$\rho = \frac{1}{2} \begin{bmatrix} P_0 + P_z & P_x - iP_y \\ P_x + iP_y & P_0 - P_z \end{bmatrix} \tag{3.11}$$

The main diagonal values of the density matrix represents the occupancy value for the two neutrino species. For now, lets assume the two species to be electron neutrino and sterile neutrino.

$$n_e = \frac{1}{2}(P_0 + P_z) \tag{3.12}$$

$$n_s = \frac{1}{2}(P_0 - P_z) \tag{3.13}$$

The off-diagonal term measure the coherence in the mixed states of the neutrinos.

3.3 Time Evolution of Density Matrix

The time evolution of the flavour density matrix can derived from the equations 3.2 and 3.3.

$$\rho(t) = e^{-iH_f t} \rho(0) e^{+iH_f t} \tag{3.14}$$

The differentiation of the 3.14 with respect to time, gives us the Liouville Equation,

$$\frac{d\rho(t)}{dt} = -iH_f \rho(t) + i\rho(t) H_f \tag{3.15}$$

or in terms of commutation operator

$$\frac{d\rho(t)}{dt} = -i[H_f, \rho(t)]. \tag{3.16}$$

The equation 3.16 can be expanded in terms of the polarization vectors in vacuum,

$$\frac{dP_0}{dt} = 0, \tag{3.17}$$

$$\frac{d\vec{P}}{dt} = \vec{V} \times \vec{P}. \tag{3.18}$$

V are the projections of H_f taken along the directions of the sigma matrices $\sigma_{x,y,z}$. When the neutrinos travel in a medium, we need to introduce the terms for scattering medium potentials in $\vec{V}$, damping and repopulation terms in the differential equations.

$$\frac{dP_0}{dt} = R_e \tag{3.19}$$

where R_e is the repopulation rate of the electron flavour neutrinos; this quantity is zero for vacuum propagation and non-zero for dense media like solar medium, early universe plasma. These terms are similar to the term in [13]

$$R_e = F_0(p)C_e\left(\frac{f(p,u)}{f(p,0)} - N_e\right) \tag{3.20}$$

F_0 is the term for collision rate of neutrino with the medium, $C_e = 1.27$ is the coefficient for electron flavour neutrinos and for muon and tau neutrinos the coefficients are $C_\mu = C_\tau = 0.92$. $f(p,u) = \frac{1}{1+e^{p/T-u}}$ is the Fermi-Dirac distribution with momentum p and chemical potential u.

After adding medium potential, Damping terms. and Repopulation terms, the equation 3.18 can be written as

$$\frac{d\vec{P}}{dt} = \vec{V}_{vac+med} \times \vec{P} - D(P_x + P_y) + \frac{dP_0}{dt}\hat{z} \tag{3.21}$$

Where D is the damping rate, taken to be half of the collision frequency. The damping takes away the coherence of the system and therefore the damping term is off-diagonal in the density matrix. The Repopulation term on the other hand is added to the main diagonal thus affecting the occupancy of the neutrino species directly.

$$D = \frac{1}{2}F_0 \tag{3.22}$$

The medium potential, damping and repopulation terms are generated by the dense medium that a neutrino travels through. These terms are explained in much detail in next two chapters. There are also some effects that originate from the evolution of matter and anti-matter together in a dense medium, which make the evolution non-linear.

4 Dense Media Effects

The media plays an important role in forward scattering. As in case for solar neutrinos, the solar medium enhances the flavour conversion by altering the coherent scattering potentials to produce resonances such that probabilities for appearance of solar neutrinos becomes independent of mixing angle [14].This phenomenon was later named the MSW effect and then the observations by SNO and Super-Kamiokande detector of the neutrino confirmed the MSW effect in solar plasma and solved the solar neutrino problem and led to the Nobel Prizes.

4.1 Primordial Dense Media

The early universe during the weak decoupling epoch only contained elementary particles with rest masses equal to or below electron's rest mass. This time period (100 MeV > T > 1 MeV) was not cool enough to produce nuclei, hence the universe contained light elementary fermions. The fermions that are neither too heavy to decay nor have low binding energy are 3 neutrinos and the electrons. The nucleon synthesis follows this period shortly; hence the imprint of the dynamics of the weak decoupling can be traced by the ratios of the light elementary particles in the present age. The primordial plasma interacts with the active neutrinos via forward scattering, mixed-state potentials, damping and repopulation of the active species. Sterile neutrinos do not feel any potential and does not undergo repopulation by pair-production.

4.2 Coherent Forward Scattering

The Neutrinos undergo scattering with the primordial plasma containing abundant low energy particles that interact with neutrinos and anti-neutrinos via the W and Z bosons. For the era of weak decoupling, the interaction with muons and heavier particles can be neglected for simplification. The three species of neutrinos experience both elastic and non-elastic scatterings with plasma contents. The neutrinos that we are interested in are the ones which conserve the coherence of the neutrino ensembles. These type of scattering are known as coherent forward scattering.

For this to happen, we need to take the reactions that have neutrinos in the initial state as well as the final state. The reactions with intermediate Z-boson are common for all 3 active-flavors. While the reactions involving $W^{\pm}$ bosons are limited to electron flavour.

The forward scattering potentials can be derived in two ways, one is to use the QFT finite-temperature Lagrangian approach as done in [15] and [16]. The other way is to use the integral over scattering amplitudes as in [17] and by Rudzsky in [18]. In both the cases the potential terms are order G_f, in the later case the potential depends on the Matrix element for scattering in a linear fashion.

4.3 Active-Sterile Potentials

The sterile neutrinos are non-interacting in weak interactions, while the active species undergo weak current interactions. Both the charged current and neutral current will contribute to the new flavour hamiltonian. For a active flavour $\alpha = e, \mu, \tau$ the active-sterile potentials just get added to the flavour hamiltonian H_f. The new flavour hamiltonian is given by :

$$H_f^{vac+med} = H_f + \delta_{\alpha\beta}(\delta_{\alpha e} V_{cc} + V_{nc}) \tag{4.1}$$

where $\beta = \alpha$ for active flavour and $\beta = s$ for sterile flavour. V_{cc} and V_{nc} are the charged and neutral current potentials from the background plasma.

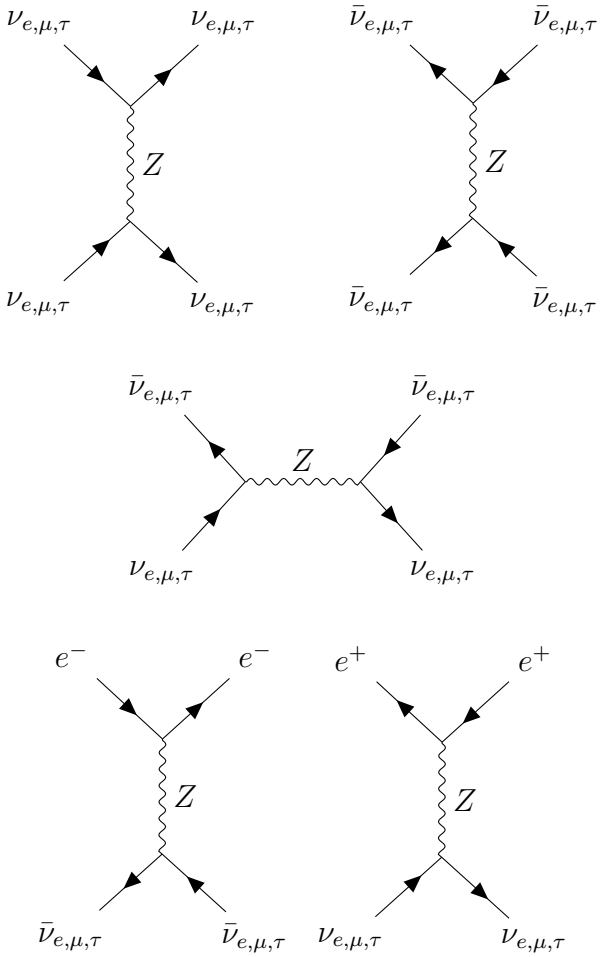

Figure 4.1: Neutral current interactions

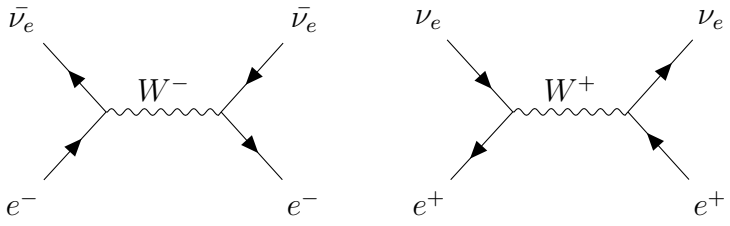

Figure 4.2: Charged current interactions

4.4 Active-Active Potentials

The charged current interactions will, however, only be limited to electron flavor neutrino for weak decoupling energy range [100 MeV to 1 MeV], as the energy is less than the mass of a muon, therefore a muon or tau lepton in the final state can't be produced on these energy scales. Hence, there would be difference between potentials of active-active species only if one species is electron flavoured. However, matter-antimatter effects also play an important role in active-active potentials.

4.5 Matter-AntiMatter Potentials

The active-active case is also different because, unlike the sterile state that could not undergo scattering, here both the species are active flavour. Thus the resultant superposition or mixed state between the two gives rise to an off-diagonal potential that can be felt by the mixed active-active states. This off-diagonal potential $V^{\alpha\beta}$ contains both mixed matter-matter and matter-anti-matter interactions.

$$H_f^{vac+med} = H_f + \delta_{\alpha\beta}(\delta_{\alpha e}V_{cc} + V_{nc}) + V^{\alpha\beta} \tag{4.2}$$

Here β only runs over active species and $V^{\alpha\beta}$ is zero for $\alpha \neq \beta$.

There are interactions between matter and anti-matter flavour eigenstates, pure state and also mixed states. The pure states can be directly influenced by introducing a potential due to lepton asymmetry in V_{cc} and V_{nc} above. This term has opposite sign for matter and anti-matter.

4.6 Damping Effects

The active flavour neutrinos also interact to background medium in ways that lead to loss of coherence via collisions. The interactions of active neutrinos to background not only creates a forward scattering potential, in which the final state contains a neutrino with conserved phases and momentum, but there are

also reaction where the phase is not conserved in the scattering process and sometimes there are no neutrinos in the final state of the scattering. These type of reactions lead to loss of coherence of the neutrino system. Damping terms are of order G_f^2 and are rate limited by the temperature, making them less effective at lower temperatures.

4.7 Repopulation effects

In the primordial plasma the background also served as pair-production driver for active flavour states producing coherent neutrino states. The rate was limited by the free states that are available for the newly generated fermions. The repopulation term used in the thesis also has a dependence on chemical potential generated by the Lepton Asymmetry. Hence the repopulation received by the neutrinos and anti-neutrinos would be different.

5 2 Active and 1 Sterile Flavour Model

5.1 2+1 flavour mixing

To write down equations for the 2+1 neutrino mixing, the density matrix formalism has been used in the flavour space. The density matrix, describing the mixed neutrinos, can be expanded in the form of polarization vectors.

$$\rho = \frac{1}{2}(P_0 + \sum_i \lambda_i P_i) \tag{5.1}$$

where λ_i are the 8 Gell-Mann matrices. After expanding the summation, the density matrix can be written as:

$$\rho = \frac{1}{2}\begin{bmatrix} P_0 + P_3 + \frac{1}{\sqrt{3}}P_8 & P_1 - iP_2 & P_4 - iP_5 \\ P_1 + iP_2 & P_0 - P_3 + \frac{1}{\sqrt{3}}P_8 & P_6 - iP_7 \\ P_4 + iP_5 & P_6 + iP_7 & P_0 - \frac{2}{\sqrt{3}}P_8 \end{bmatrix} \tag{5.2}$$

Here the diagonal values of the matrix represents the values of normalised number densities of the 3 flavours of neutrino species.

$$n_e = \frac{1}{2}(P_0 + P_3 + \frac{1}{\sqrt{3}}P_8) \tag{5.3a}$$

$$n_\mu = \frac{1}{2}(P_0 - P_3 + \frac{1}{\sqrt{3}}P_8) \tag{5.3b}$$

$$n_s = \frac{1}{2}(P_0 - \frac{2}{\sqrt{3}}P_8) \tag{5.3c}$$

Here the reader can assess the structure of the equation 5.2 and see that the 2x2 sigma matrices formulation can be derived by setting P_8 and cross elements between the active sterile species to zero.

The mixing matrix U for 3 flavour basis is

$$U = \begin{bmatrix} c_{12}c_{13} & c_{13}s_{12} & s_{13} \\ -c_{12}s_{13}s_{23} - c_{23}s_{12} & c_{12}c_{23} - s_{12}s_{13}s_{23} & c_{13}s_{23} \\ -c_{12}c_{23}s_{13} + s_{12}s_{23} & -c_{12}s_{23} - c_{23}s_{12}s_{13} & c_{13}c_{23} \end{bmatrix} \tag{5.4}$$

where c_{ij} and s_{ij} are $cos(\theta_{ij})$ and $sin(\theta_{ij})$ respectively, and θ_{ij} are the mixing angles. The CP-violating phase has been ignored from the mixing matrix to keep the derivation simple.

The Vacuum Potential H_f in flavour space will have similar expansion with Gell-Mann matrices as of the polarization vector. We know the flavour Hamiltonian $H_f = UH_mU^\dagger$, with $H_m = diag(m_1^2, m_2^2, m_3^2)/2E$

$$H_f = \begin{bmatrix} H_0 + H_3 + \frac{1}{\sqrt{3}}H_8 & H_1 - iH_2 & H_4 - iH_5 \\ H_1 + iH_2 & H_0 - H_3 + \frac{1}{\sqrt{3}}H_8 & H_6 - iH_7 \\ H_4 + iH_5 & H_6 + iH_7 & H_0 - \frac{2}{\sqrt{3}}H_8 \end{bmatrix} \tag{5.5}$$

Here, except for H_0 which is $(m_1^2 + m_2^2 + m_3^2)/6E$, solving for each of the other eight components of the H_i vector will yield forms as following.

$$H_i = k_{i1}\frac{m_1^2}{2E} + k_{i2}\frac{m_2^2}{2E} + k_{i3}\frac{m_3^2}{2E} \tag{5.6}$$

where k_{i1} are some numerical values that may seem complicated but the δm_{ij}^2 can be recovered by knowing that, k_{i2} will always be $-(k_{i3} + k_{i1})$.

$$H_i = -k_{i1}\frac{\delta m_{12}^2}{2E} - k_{i3}\frac{\delta m_{23}^2}{2E} \tag{5.7}$$

5.2 Quantum Kinetic Equation for 2+1 flavour model

Now, to write out the evolution of the mixed neutrino density matrix we start by taking time derivative of Equation 5.1, which will yield in a commutator product containing Gell-Mann matrices.

$$i\frac{\partial P_k \cdot \lambda_k}{\partial t} = [H_i \cdot \lambda_i, P_j \cdot \lambda_j] \tag{5.8}$$

Here, we can use the $SU(3)$ structure constant $\mathcal{F}_{ijk}$ to get rid of all λ's, Note that the structure used here is twice the original one.

$$\frac{\partial P_k}{\partial t} = H_i P_j \mathcal{F}_{ijk} \tag{5.9}$$

Now, we add potential terms for 2 different active neutrino species to the vacuum terms.

$$V_e = -\frac{7\pi^2 G_f x T^5}{45\sqrt{2}M_z^2}(\mathcal{N}_e + \mathcal{N}_{\bar{e}} + 5.143) + \frac{2\sqrt{2}\zeta(3)}{\pi^2} G_f T^3 L_e \tag{5.10}$$

$$V_\mu = -\frac{7\pi^2 G_f x T^5}{45\sqrt{2}M_z^2}(\mathcal{N}_\mu + \mathcal{N}_{\bar{\mu}}) + \frac{2\sqrt{2}\zeta(3)}{\pi^2} G_f T^3 L_\mu \tag{5.11}$$

where $\mathcal{N}_\alpha$ is the number density normalized to unity, given by

$$\mathcal{N}_\alpha = \frac{2}{3\zeta(3)}\int (n_\alpha) f_0(x) x^2 dx \tag{5.12}$$

where the first term for both species is the coupling to background plasma, and the second term is the correction for lepton asymmetry between the matter and anti-matter particles of same flavours. The potential for electron neutrino also contains contribution from charged current interactions i.e. 5.143 term. Here $L_e = n_e - n_{\bar{e}}$ and $L_\mu = n_\mu - n_{\bar{\mu}}$ are the active neutrino asymmetries. As pointed out in [19], as well as in [20], there are also off-diagonal terms due to active oscillations adding up to the potential experienced by the two species.

$$V^{e\mu} = \frac{\sqrt{2}G_f\zeta(3)T^3}{4\pi^2}\left\{[(P_1 + iP_2) - (\bar{P}_1 + i\bar{P}_2)] - \frac{28\zeta(4)T}{3\zeta(3)M_z^2}(P_1 + iP_2)\right\} \tag{5.13}$$

The bars over polarization vectors indicate that they represent the anti-matter species. While setting the lepton asymmetry to zero, one must remember that the part inside square brackets in the above equation would go to zero.
The second term with $(P_1 + iP_2)$ is the first order QFT correction and decays as mass squared of the carrier **Z** boson, this term is 10^{-15} order smaller compared to the first term, it can be neglected without the loss of much precision. There is an additional term for anti-matter [21] which looks similar to the last term, and is neglected for same reason.

We now have to add these 3 terms to correct H_i terms and write the full effective potential vector V_i. This can be easily done by calculating differences in potential felt by two active species as compared to sterile species, in terms of V_i's, and then equating them to the defined potentials above. We get the following:

$$V_1 = H_1 + real(V^{e\mu}) \tag{5.14a}$$

$$V_2 = H_2 - imag(V^{e\mu}) \tag{5.14b}$$

$$V_3 = H_3 + \frac{1}{2}(V_e - V_\mu) \tag{5.14c}$$

$$V_8 = H_8 + \frac{1}{2\sqrt{3}}(V_e + V_\mu) \tag{5.14d}$$

V_4, V_5, V_6, V_7 will remain the same as H_4, H_5, H_6, H_7, as the diagonal terms between active-sterile species combinations receive no additional potential from the plasma. This happens because the scattering matrix for mixed active-sterile neutrinos would contains a final state with mixed active-sterile state and contraction of such state vectors would be zero in case of non self-interacting sterile neutrinos.

5.2.1 Damping and Repopulation Terms

The early universe before the weak decoupling of neutrinos was dominated by primordial plasma, which affects the mixed neutrino states by introducing decoherence(damping), coupling matter with anti-matter and refilling of empty states created by oscillation to sterile flavour (repopulation). These terms can be derived via values from the table in [19], along with the approximation that the active neutrino system is kept in thermal equilibrium. This condition requires the rate of weak reactions to be greater than the rate of oscillations,

which is already satisfied in the weak epoch (100 MeV to 1 MeV). To make it suitable for the multi-momentum approach, the damping and repopulation rates for each comoving momenta points have been calculated individually and the background parameters like lepton asymmetries and N_{eff} are integrated over the momentum space. There would be refilling of both ν_e and ν_μ that would be added to the diagonal elements of the density matrix derivatives.

$$R_e = G_f^2 x T^5 C_e \left(\frac{f(p,u)}{f(p,0)} - n_e \right) \tag{5.15}$$

$$R_\mu = G_f^2 x T^5 C_\mu \left(\frac{f(p,u)}{f(p,0)} - n_\mu \right) \tag{5.16}$$

Here, the first terms is just the re-population rate of the background plasma to the corresponding neutrino flavours with $C_e = 1.27$ and $C_\mu = 0.92$. The term is of order G_f^2 as it arise from 2 vertex interactions with the background.
Next, the system of evolution equations can described as following.

$$\frac{d}{dt} P_0 = \frac{2}{3}(R_e + R_\mu) \tag{5.17}$$

$$\frac{d}{dt} P_3 = V_i P_j \mathcal{F}_{ij3} + (R_e - R_\mu) \tag{5.18}$$

$$\frac{d}{dt} P_8 = V_i P_j \mathcal{F}_{ij8} + \frac{1}{\sqrt{3}}(R_e + R_\mu) \tag{5.19}$$

The zeroth element of the polarization vector only receives contribution from the repopulation terms. While the third and eighth term are contain not only combinations of refilling R_e and R_μ, but also of the contraction between the potential vector, polarization vector and the structure constant, which is a rank 3 tensor. These 3 terms lie on the main diagonal and are responsible for adding and removing neutrinos to the 3 flavours via both weak reactions as well as oscillations. Similarly, the other 6 equations are also a combination of damping (decoherence) terms and contraction between the aforementioned vectors and tensors.

$$\frac{d}{dt} P_4 = V_i P_j \mathcal{F}_{ij4} - D_e P_4 \tag{5.20}$$

$$\frac{d}{dt} P_5 = V_i P_j \mathcal{F}_{ij5} - D_e P_5 \tag{5.21}$$

where $D_e = 0.635\ G_f^2 x T^5$.

$$\frac{d}{dt} P_6 = V_i P_j \mathcal{F}_{ij6} - D_\mu P_6 \tag{5.22}$$

$$\frac{d}{dt}P_7 = V_i P_j \mathcal{F}_{ij7} - D_\mu P_7 \tag{5.23}$$

where $D_\mu = 0.46\ G_f^2 x T^5$.

$$\frac{d}{dt}P_1 = V_i P_j \mathcal{F}_{ij1} - D' P_1 - C' \bar{P}_1 \tag{5.24}$$

$$\frac{d}{dt}P_2 = V_i P_j \mathcal{F}_{ij2} - D' P_2 - C' \bar{P}_2 \tag{5.25}$$

where $D' = 0.625\ G_f^2 x T^5$ and $C' = 0.39\ G_f^2 x T^5$. There are 4 different damping coefficients, each affecting specific cross diagonal terms between 2 neutrino species. D_e and D_μ are the the damping terms between the electron neutrino and the sterile species, and between the muon neutrino and the sterile species respectively. D' is the active-active damping parameter between electron and muon neutrinos, and C' dictates the annihilation between mixed electron-muon neutrino species of matter and anti-matter.

5.3 Evolution of Lepton Asymmetry

The Effective Lepton Asymmetry is defined as

$$L_\alpha = L_0 + 2L_{\nu_\alpha}. \tag{5.26}$$

The term L_0 is the initial asymmetry due to neutrons, protons and electrons and is taken to be 10^{-10}, L_α is the effective asymmetry in ν_α flavour of neutrinos and is used to make notations easier.

$$L_{\nu_\alpha} = \frac{3}{8}\left[n_\alpha - n_{\bar{\alpha}}\right] \tag{5.27}$$

Lepton asymmetry L_α is a quantity getting affected by the refilling of states, however, this refilling is different for matter and anti-matter. This leads to lepton number violation in this process. In order to conserve the lepton number, the derivative of the lepton asymmetry can be defined with only oscillation terms and repopulation and damping terms do not enter into the derivative.

$$\frac{dL_\alpha}{dt} = \frac{1}{4\zeta(3)}\int (\dot{n}_\alpha - \dot{n}_{\bar{\alpha}}) f_0(x) x^2 dx \tag{5.28}$$

$$\frac{dL_e}{dt} = \frac{1}{4\zeta(3)} \int \frac{1}{2} \left[(V_i P_j - \bar{V}_i \bar{P}_j) \mathcal{F}_{ij3} + \frac{1}{\sqrt{3}} (V_i P_j - \bar{V}_i \bar{P}_j) \mathcal{F}_{ij8} \right] f_0(x) x^2 dx \tag{5.29}$$

$$\frac{dL_\mu}{dt} = \frac{1}{4\zeta(3)} \int \frac{1}{2} \left[-(V_i P_j - \bar{V}_i \bar{P}_j) \mathcal{F}_{ij3} + \frac{1}{\sqrt{3}} (V_i P_j - \bar{V}_i \bar{P}_j) \mathcal{F}_{ij8} \right] f_0(x) x^2 dx \tag{5.30}$$

The chemical potential u can be calculated from the definition of lepton asymmetry at equilibrium, as done in [13].

$$u = \frac{-2\pi}{\sqrt{3}} sinh \left(\frac{1}{3} arcsinh \left[\frac{-18\sqrt{3}\zeta(3) L_\alpha}{\pi^3} \right] \right) \tag{5.31}$$

5.3.1 Evolution equations for Anti-Neutrinos

The anti-neutrinos experience the same potential from the plasma, except for the terms containing lepton asymmetry and the active-active potentials. The potential terms for anti-neutrinos $V_{\bar{e}}$, $V_{\bar{\mu}}$ and $V_{\bar{e}\bar{\mu}}$ can be derived by setting $L \rightarrow -L$ and $P_1 \& P_2 \rightarrow \bar{P}_1 \& \bar{P}_2$. The chemical potential in the distribution function is $\bar{u} = -u$ for anti-neutrinos.

5.4 Evolution with Temperature

In an expanding Universe we need a different variable to describe momentum of mixed neutrinos. Various studies have used the co-moving momentum $x = p/T$ as the variable of choice and evolved it over temperature instead of time. The time-temperature relationship can be derived by considering the temperature T of a photon moving through early expanding universe of wavelength a in it's co-moving frame.

$$a \propto \frac{1}{T} \tag{5.32}$$

And the Hubble parameter $\mathcal{H}$, is defined as:

$$\mathcal{H} = \frac{\dot{a}}{a} \tag{5.33}$$

Substituting equation (4.8) in (4.9), we get

$$\frac{\partial t}{\partial T} = -\frac{1}{\mathcal{H}T} \tag{5.34}$$

Then, by using the Friedmann equations for weak-decoupling epoch, we have

$$\mathcal{H}(T) = \sqrt{\frac{8\pi^3 g_b G T^4}{45}} \tag{5.35}$$

$$g_b = \frac{43}{8} + \frac{7}{8} N_{eff} \tag{5.36}$$

Where g_b is the total number of degrees of freedom, and N_{eff} is the number of effective degrees of freedom from all neutrinos. The value for N_{eff} can be calculated by,

$$N_{eff} = \frac{\Sigma_\alpha \int n_\alpha f_0(x) x^3 dx}{\int f_0(x) x^3 dx} \tag{5.37}$$

where $f_0(x) = 1/(1 + e^x)$ is the Fermi-Dirac function with zero chemical potential.For reducing the computation time, the value of N_{eff} is set to 3 in the equation 5.36. Using equation (4.27) we can write the temperature derivative in terms of time derivative.

$$\frac{\partial}{\partial T} = \frac{\partial}{\partial t}\frac{\partial t}{\partial T} = -\frac{1}{\mathcal{H}T}\frac{\partial}{\partial t} \tag{5.38}$$

5.4.1 Effective Degrees of Freedom, N_{eff}

N_{eff}, the number of effective degrees of freedom is a cosmological quantity of interest, which is defined as degrees of freedom from non-radiation content. In relevance to the thesis the quantity ΔN_{eff} measures the degrees of freedom generated by the sterile neutrino production and repopulation of the free energy states in the fermi-distribution of the neutrinos.

5.5 Commutator Values by Expanding Einstein Summations

The values for the commutator in the 2+1 flavour model are given as the following Einstein summation over potential, polarization vector, and the SU(3) structure constant $\mathcal{F}_{ijk}$.

$$V_i P_j \mathcal{F}_{ij1} = -P_2 V_3 + P_3 V_2 + \frac{1}{2} P_5 V_6 + \frac{1}{2} P_7 V_4 \tag{5.39a}$$

$$V_i P_j \mathcal{F}_{ij2} = P_1 V_3 - P_3 V_1 - \frac{1}{2} P_4 V_6 + \frac{1}{2} P_6 V_4 \tag{5.39b}$$

$$V_i P_j \mathcal{F}_{ij3} = -P_1 V_2 + P_2 V_1 + \frac{1}{2} P_5 V_4 - \frac{1}{2} P_7 V_6 \tag{5.39c}$$

$$V_i P_j \mathcal{F}_{ij4} = \frac{1}{2} P_2 V_6 - \frac{1}{2} P_6 V_2 - \frac{1}{2} P_7 V_1 - \frac{1}{2} (V_3 + \sqrt{3} V_8) P_5 \tag{5.39d}$$

$$\begin{aligned} V_i P_j \mathcal{F}_{ij5} = -\frac{1}{2} P_1 V_6 + \frac{1}{2} P_6 V_1 - \frac{1}{2} P_7 V_2 - \frac{1}{2} (P_3 + \sqrt{3} P_8) V_4 \\ + \frac{1}{2} (V_3 + \sqrt{3} V_8) P_4 \end{aligned} \tag{5.39e}$$

$$V_i P_j \mathcal{F}_{ij6} = -\frac{1}{2} P_2 V_4 + \frac{1}{2} P_4 V_2 - \frac{1}{2} P_5 V_1 - \frac{1}{2} (-V_3 + \sqrt{3} V_8) P_7 \tag{5.39f}$$

$$\begin{aligned} V_i P_j \mathcal{F}_{ij7} = -\frac{1}{2} P_1 V_4 + \frac{1}{2} P_4 V_1 + \frac{1}{2} P_5 V_2 - \frac{1}{2} (-P_3 + \sqrt{3} P_8) V_6 \\ + \frac{1}{2} (-V_3 + \sqrt{3} V_8) P_6 \end{aligned} \tag{5.39g}$$

$$V_i P_j \mathcal{F}_{ij8} = \frac{\sqrt{3}}{2} P_5 V_4 + \frac{\sqrt{3}}{2} P_7 V_6 \tag{5.39h}$$

The values for vacuum potentials V_2, V_5, and V_7 are all zero for the entire temperature range. However, the active-active potential 5.13 adds to the vacuum value of V_2 leading to a non-zero value.

6 Numerical Simulations and Results

6.1 Details of Numerical Computation

The primary version of the code is written in python, and scipy ODE solver, with the method set to **dopri5**, was used to solve the differential equations, it is based on Runge-Kutta method of order 4-5. Other solver, based on Range-Kutta of order 5, **dop853**, was used to check for the solver dependence of solution. Both solvers are written in Fortran with Python wrapper built around them, they both converged on the solution with dop853 being slower than dopri5. To speed up the solution convergence numpy module was used for doing all the matrix and linear algebra operations. It allows for the array operations to be offloaded from python to C/C++ where it can be executed better at machine level. Checks for convergence were also done using different tolerances and increasing comoving momentum bins, both of which showed small dependencies on these parameter, however, there was no significant deviation of the overall trend of the output from the solver.

6.2 Numerical Evolution of Density Matrix 1+1 model

The above defined evolution equations are defined such that they can be solved for both average momentum and multi-momentum evolution with minimum changes required. The model used above is good for simulating both 2+1, as

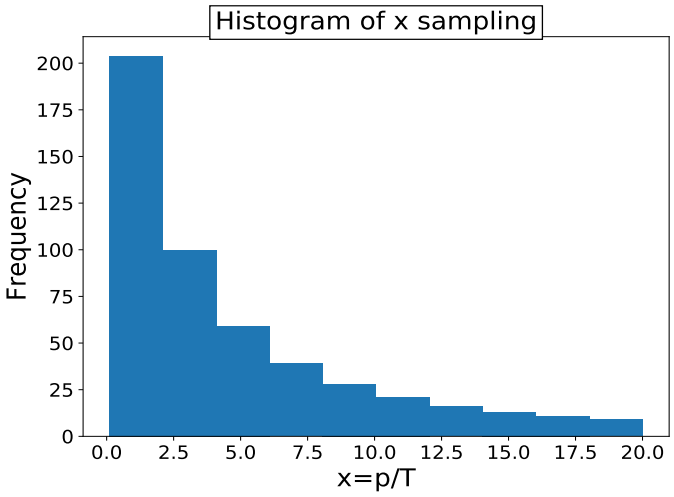

Figure 6.1: Distribution of sampled comoving momentum 'x' points

well as, 1+1 mixing with one sterile species. In the following subsections the results from 1+1 multi-momentum model are presented.

6.2.1 1+1 Flavour model with Zero Asymmetry

For testing the workings of the evolution equations, it is first tested with 1+1 flavour model with zero lepton asymmetry based on [13], for single and multi-momentum output simulations. For multi-momentum runs, it's needed to track the motion of resonance through the spectrum. To accomplish this task comoving momentum grid is defined like [22], but with different $x_{min} = 10^{-2}$, $x_{max} = 20$ and $x_{ext} = 3.15$, and with 500 points. The fig. 6.1 shows the histogram of distribution of selected x-points.

The reduction of of 2+1 model to 1+1 model requires a few things, one is selecting an active flavour, here muon neutrino was chosen and setting the mixing angles and squared mass difference for the other active species to be set to zero, i.e. $\theta_{12} = 0$, $\theta_{13} = 0$ and $\delta m^2_{12} = 0$. Here the mixing angle is taken to be $\theta_{23} = 0.0184$ and separation between mass eigenstates $\delta m^2_{23} = -3 \times 10^{-3} eV$. The system was evolved from 20 MeV to 1 MeV (electron-positron annihilation). It is a case for Inverted Hierarchy (IH) where the δm_{23} is negative, hence the vacuum frequency can be equated by the effects of media and lead to MSW resonances. The resonances are both momentum and temperature dependent, therefore the entire spectrum will not go into resonance simultaneously.

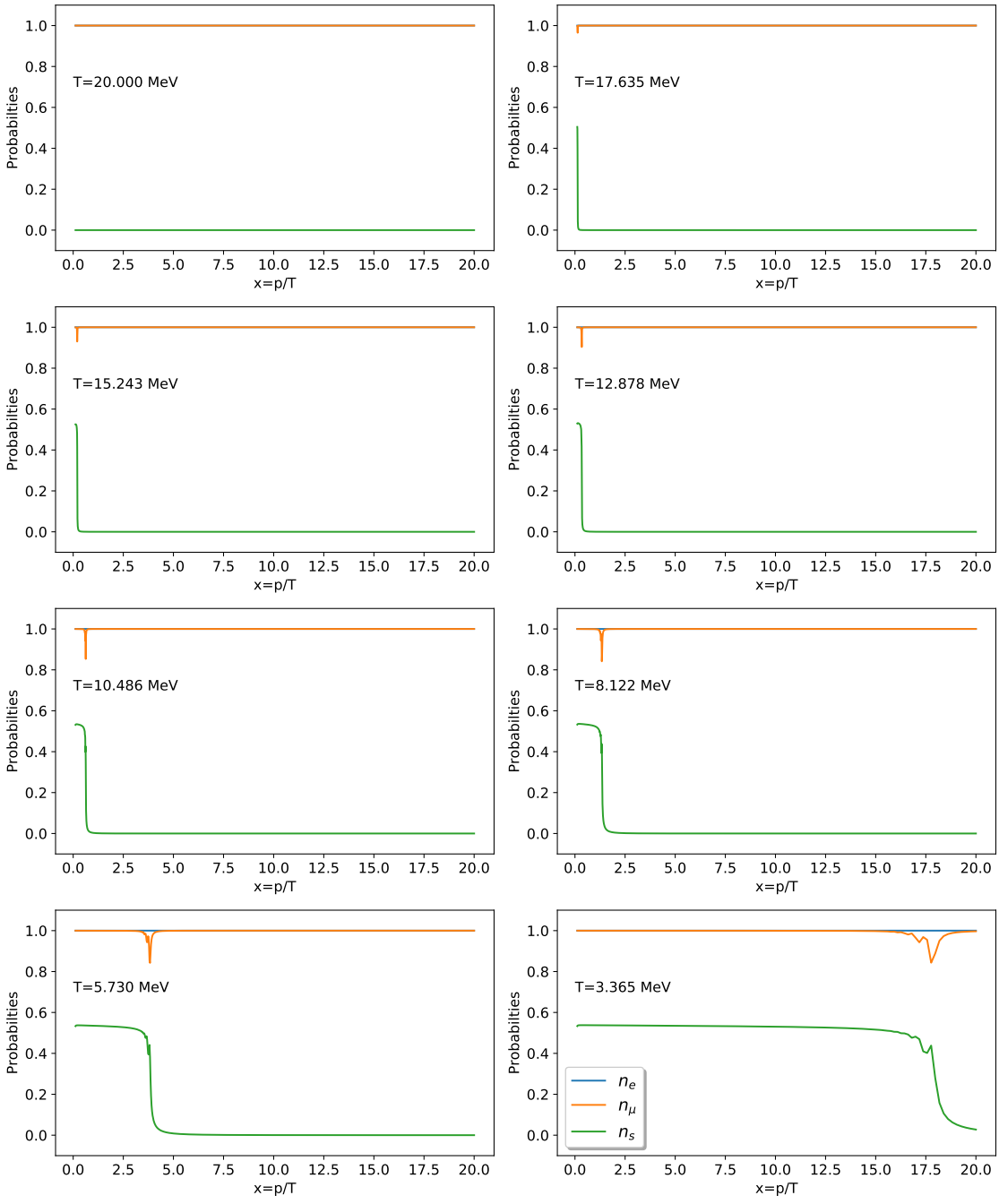

Figure 6.2: Evolution of normalised population of ν_e, ν_μ and ν_s with $s_{23} = 0.0184$ and $\delta m^2_{23} = -3 \times 10^{-3} eV$ and $L_\mu = 0$.The system was evolved numerically from temperature 20 MeV to 1 MeV. Blue curve for electron neutrinos is under the orange curve.

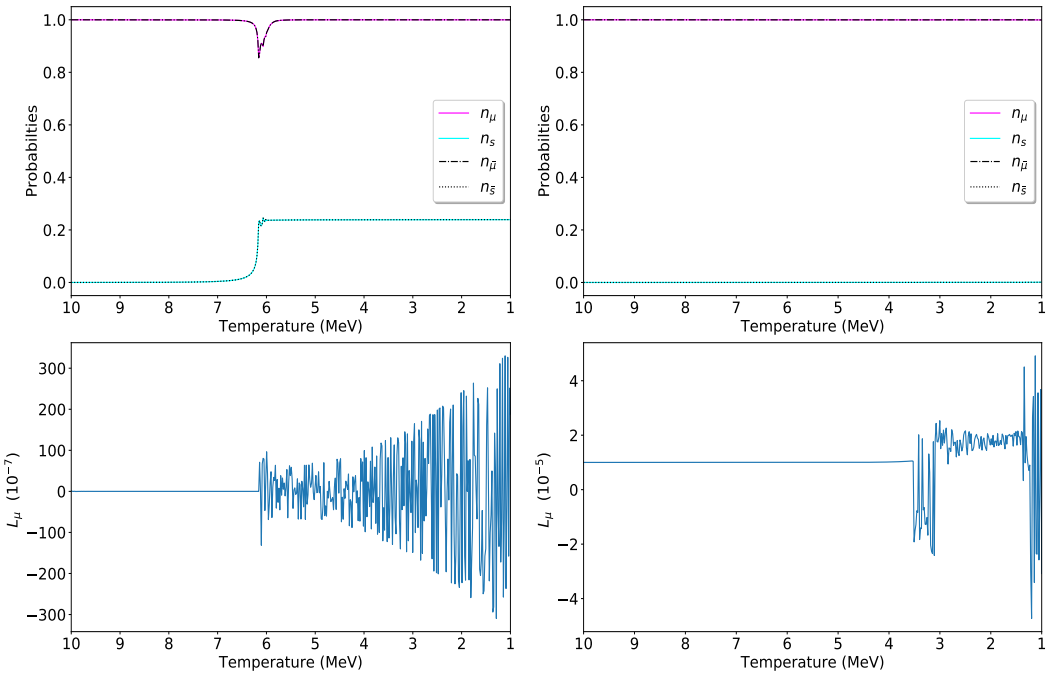

(a) $L_\mu = 10^{-7}$ **(b)** $L_\mu = 10^{-5}$

Figure 6.3: The Evolution of 1+1 model with initial lepton asymmetry $L_\mu = 10^{-7}$ and $L_\mu = 10^{-5}$

It can be seen from fig. 6.2, the electron neutrinos remains unaffected by mixing between muon and the sterile flavours, i.e. the parameters set have reduced the 2+1 flavour model to 1+1 model effectively. Here the resonances between the selected flavour and sterile neutrinos can seen moving through the momentum space as the temperature is going down. The oscillation between the two flavours is bringing the sterile neutrinos into thermal contact with the universe. The thermalisation for this case brings the entire spectrum of sterile neutrinos in thermal contact with the background plasma before the neutrino decoupling. However this will not be the case always and there can be partial thermalisation of the sterile species and resonances can occur after the electron-positron annihilation(1 MeV), this model does not account for photon reheating due to recombination.

6.2.2 1+1 Flavour model with Non Zero Asymmetry

The fig. 6.3 shows the evolution 1+1 model along with anti-neutrinos and the second panel show the evolution of lepton asymmetry, Here the parameters for evolution were same as the zero lepton asymmetry case, except the initial lepton asymmetry $L_\mu = 10^{-7}$ and 10^{-5}. This system was evolved from 10 MeV to 1 Mev. Since the repopulation terms are not present in the derivative of lepton asymmetry the changes in this quantity can only be driven by the oscillation to sterile neutrinos(anti-neutrinos).
The Lepton Asymmetry seems to always jump to order of 10^{-5} for values less than 10^{-5}, while for initial value above 10^{-5} the value for lepton asymmetry stay in order of the 10^{-5}.

6.2.3 1+1 Model Evolution for Positive Δm^2

The simulations for this subsection were run with 100 momentum points on the grid over 8000 temperature points from 60 MeV to 1 MeV.

In figure 6.4 the value for 1+1 model for electron-sterile flavours (blue curves) and muon-sterile flavours(orange curves) has been plotted for their evolutions from 60 MeV to 1 MeV. For the range of combinations for both mixing angles e-s(θ_{13}) and μ-s(θ_{23}) and mass difference splittings between active-sterile flavours Δm^2 show a decrease in value of the asymmetries, all the features for the asymmetries lie under 10^{-10} dashed black line. To suppress the production of sterile neutrinos significantly the value of the Lepton Asymmetry should be higher depending on the mixing parameter values and potentials due to media. In this case, the potentials due to primordial plasma is larger than the asymmetry potential throughout the temperature range for evolution thus the evolution of N_{eff} is not greatly affected by the small asymmetry values.

In case of two flavours it's easy to track the derivatives of lepton asymmetry, since only the terms from the commutators from matter and anti-matter are the one contributing to the their evolution, it's possible to write a compact

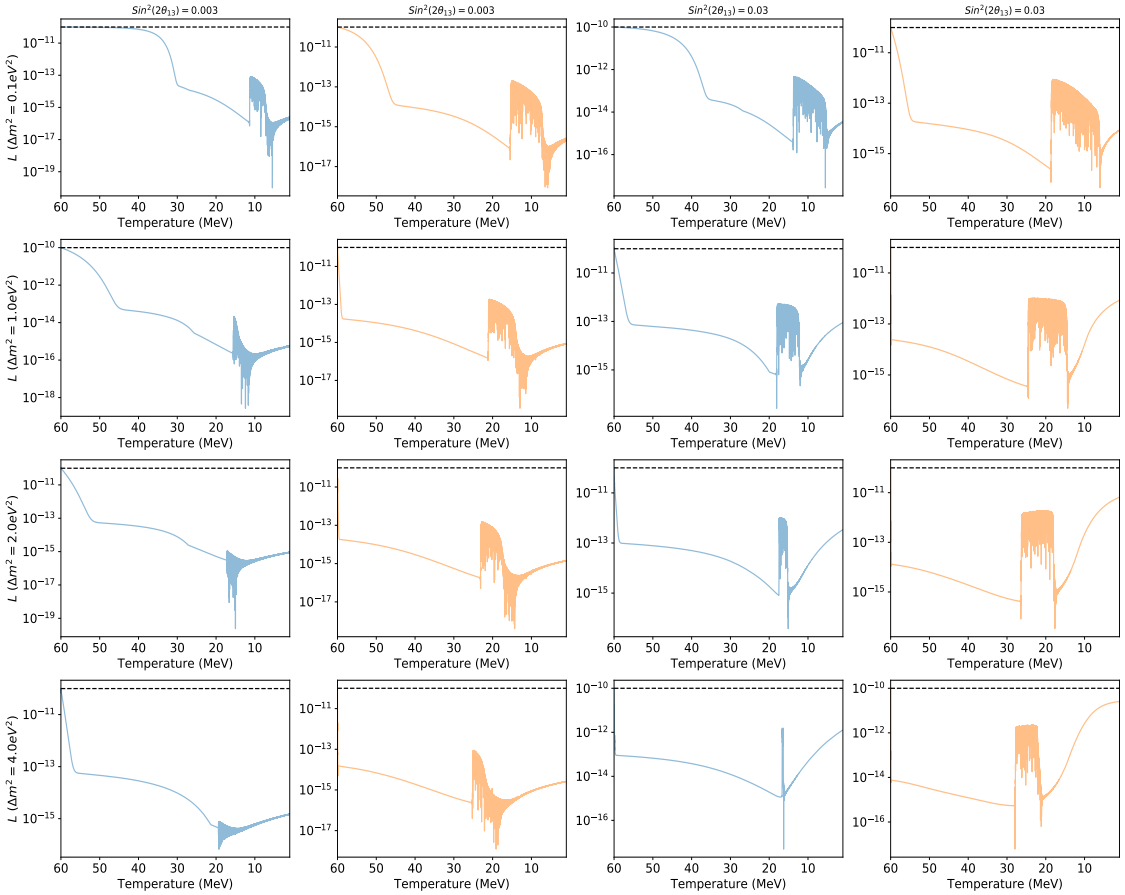

Figure 6.4: Evolution of Lepton Asymmetries for 1+1 flavour model with 100 momentum grid points. Blue color represents the asymmetry for electron flavour and orange curve represents the lepton asymmetry for muon flavour. The first row shows evolution for $\Delta m^2 = 0.1\ eV^2$, second row $\Delta m^2 = 1\ eV^2$, third row $\Delta m^2 = 2\ eV^2$ and fourth row $\Delta m^2 = 4\ eV^2$. The system was evolved from 60 MeV to 1 MeV for $sin^2(2\theta_{13})$ and $sin^2(2\theta_{23})$ written on top. The initial Asymmetry for both active flavours was taken to be 10^{-10}.

equation in terms of $P_i^{\pm} = P_i \pm \bar{P}_i$ vectors and their first order derivatives. For more simplicity we can define dP_e^- and dP_μ^- using equations 5.39

$$dP_e^- = dP_3^- + \frac{1}{\sqrt{3}} dP_8^- = P_5^- V_4 \tag{6.1}$$

$$dP_\mu^- = -dP_3^- + \frac{1}{\sqrt{3}} dP_8^- = P_7^- V_6 \tag{6.2}$$

It is further possible to look at the evolution of P_5^- and P_7^- using equations 5.39, ignoring damping terms dP_5^- and dP_7^- can be written as

$$dP_5^- = -\frac{1}{2}(P_3^- + \sqrt{3}P_8^-)V_4 + \frac{1}{2}(H_3 + \sqrt{3}H_8 + V_W + V_Z)P_4^- + \frac{1}{2}(V_{L_e})P_4^+ \tag{6.3}$$

$$dP_7^- = -\frac{1}{2}(-P_3^- + \sqrt{3}P_8^-)V_6 + \frac{1}{2}(-H_3 + \sqrt{3}H_8 + V_Z)P_6^- + \frac{1}{2}(V_{L_\mu})P_6^+ \tag{6.4}$$

Here V_W and V_Z are the forward scattering potentials due to charged and neutral current respectively.

In figure 6.4 there is a small sharp increase in asymmetries near 20 MeV, the reason for this can be inferred from the equation 6.3 where the first V_4 and P_4^- terms cancel out each other leading to increase in contribution from the P_4^+ term which depends on the asymmetric potential for electron flavour and the sharp increase is seen in the asymmetry for electron flavour, and since the value of asymmetry is small the increment of asymmetry is comparably small as well. Similarly, the first 2 terms of equation 6.4 cancel leading to the increase in variation of muon flavour asymmetry L_μ. All of this can be explained physically conditions where vacuum potential V_4 is surpassed by the potential due to primordial media V_W and V_Z. Hereafter, the fluctuations due to asymmetric potentials continue until a significant part band of charged current in taken over the vacuum potentials. If the conditions are met earlier and at higher L_e and L_μ the fluctuation region would be of short duration as higher asymmetry potential would equilibrate the entire momentum band faster. After the fluctuations the increase in lepton asymmetry is driven by vacuum and asymmetric terms.

The N_{eff} plots in figure 6.5 for 1+1 model shows that the thermalisation of sterile neutrino with muon flavour take place at lower mixing parameters as compared to electron flavoured neutrinos. This is due to the higher media potential experienced by the electron flavour due to primordial plasma.

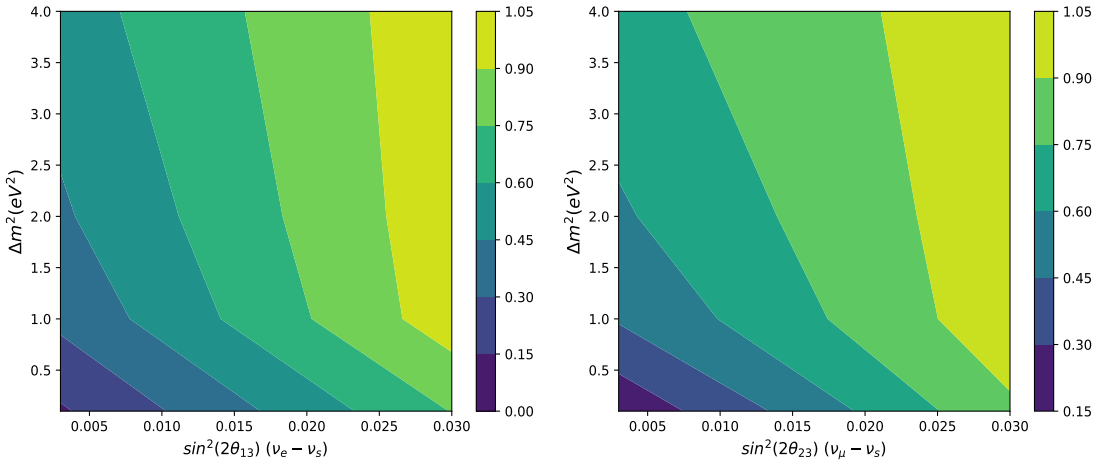

Figure 6.5: Final ΔN_{eff} for 1+1 flavour model with 100 momentum bins. The first panel is for electron-sterile flavour neutrino oscillations and second panel is for muon-sterile flavour oscillations. The system was evolved from 60 MeV to 1 MeV. The initial Asymmetry for both active flavours was taken to be 10^{-10}.

6.3 Numerical Evolution of 2+1 model

The addition of active-active mixing along with active-sterile mixing introduces new off-diagonal complex quantities which did not exist in 1+1 active-sterile case. The higher mixing angle between the active-active species also plays a significant role in the evolution of the 3 neutrino system. Henceforth for simplicity, the Δm^2 will be referred as the muon-sterile mass squared difference between muon and sterile flavour neutrinos, and the electron-muon mass squared difference and θ_{12} are fixed to $7.6 \times 10^{-5} eV^2$ and $33.45°$ respectively for all the results below. The comoving grid is also changed to $x_{min} = 10^{-1}$, $x_{max} = 50$ and $x_{ext} = 3.15$.

6.4 Dynamics of N_{eff}

The degrees of freedom N_{eff} are dependent on the sum of values P_0 and $\bar{P}_0$. This can be seen by adding the three flavours populations.

$$n_e + n_\mu + n_s = \frac{3}{2} P_0 \tag{6.5}$$

Then the equation 5.37 can be written in terms of polarisation vectors

$$N_{eff} = \frac{\int \frac{3}{2}(P_0 + \bar{P}_0) f_0(x) x^3 dx}{2 \int f_0(x) x^3 dx} \tag{6.6}$$

And the fractional degrees of freedom can be calculated by subtracting 4 from the numerator.

$$\Delta N_{eff} = \frac{\int \frac{3}{2}((P_0 + \bar{P}_0) - 4) f_0(x) x^3 dx}{2 \int f_0(x) x^3 dx} \tag{6.7}$$

If there are some unfilled active states left at the end of the run there can effective degree of freedom due to active species can be different from 4. Then to calculated degrees of freedom due to sterile species one has to use.

$$N_{eff,s} = \frac{\int \frac{3}{2}((P_0 + \bar{P}_0) - (n_e + n_{\bar{e}} + n_\mu + n_{\bar{\mu}})) f_0(x) x^3 dx}{2 \int f_0(x) x^3 dx} \tag{6.8}$$

It can be easily seen from the above formulas the evolution of all the above quantities is dependent on the addition of matter and antimatter main-diagonal terms. The 2 in the denominator is to normalize the total degrees of freedom from each matter+anti-matter pair of flavours to unity .

6.5 Dynamics of Lepton Asymmetries

The 2+1 model is essentially 3 oscillating system coupled together, therefore just looking at main diagonal potentials would not give us the full picture. There are regions of temperature that show domination of one type of oscillation and in some regions of there is interplay between two systems. The off-diagonal potential $V^{e\mu}$ is a complex quantity and a term that links matter-antimatter, along with the Lepton asymmetry potentials along the main diagonal, therefore it is useful to take a look at it, when considering to make sense of the lepton asymmetry evolution. For figuring out dynamics of L_e and L_μ the differences between matter-antimatter potentials is what taken into consideration. The dynamics of the lepton asymmetries are dependent on the differences between the derivatives of the components P_3, $\bar{P}_3$ and P_8, $\bar{P}_8$. This is due to the fact that the evolution of asymmetries conserves lepton

number and ignores the terms containing any repopulation, damping and terms involving non-vacuum potentials.

$$dP_3^- = \left[(P_2V_1 - P_1V_2) + \frac{1}{2}P_5V_4 - \frac{1}{2}P_7V_6\right] - \left[(\bar{P}_2\bar{V}_1 - \bar{P}_1\bar{V}_2) + \frac{1}{2}\bar{P}_5\bar{V}_4 - \frac{1}{2}\bar{P}_7\bar{V}_6\right] \tag{6.9}$$

$$dP_8^- = \left[\frac{\sqrt{3}}{2}P_5V_4 + \frac{\sqrt{3}}{2}P_7V_6\right] - \left[\frac{\sqrt{3}}{2}\bar{P}_5\bar{V}_4 + \frac{\sqrt{3}}{2}\bar{P}_7\bar{V}_6\right] \tag{6.10}$$

The value of above polarization vectors can also be written in terms on addition or subtraction of matter and anti-matter terms $P_i^{\pm} = P_i \pm \bar{P}_i$, the ones interesting are the P_i^- because they are related to Lepton asymmetries and are to be tracked for their evolution.

$$dP_3^- = -(P_1V_2 - \bar{P}_1\bar{V}_2) + (P_2V_1 - \bar{P}_2\bar{V}_1) + \frac{1}{2}P_5^-V_4 - \frac{1}{2}P_7^-V_6 \tag{6.11}$$

$$dP_8^- = \frac{\sqrt{3}}{2}P_5^-V_4 + \frac{\sqrt{3}}{2}P_7^-V_6 \tag{6.12}$$

V_1 and V_2 can be expressed in terms of the vacuum and medium dependent parts leading to further simplification of first two term of 6.11

$$dP_3^- = P_1^+ imag(V^{e\mu}) + P_2^- H_1 + P_2^+ real(V^{e\mu}) + \frac{1}{2}P_5^-V_4 - \frac{1}{2}P_7^-V_6 \tag{6.13}$$

The difference between the matter and anti-matter terms for electron and muon flavours asymmetry evolution can be written as

$$dP_e^- = P_1^+ imag(V^{e\mu}) + P_2^- H_1 + P_2^+ real(V^{e\mu}) + P_5^-V_4 \tag{6.14}$$

$$dP_\mu^- = -P_1^+ imag(V^{e\mu}) - P_2^- H_1 - P_2^+ real(V^{e\mu}) + P_7^-V_6 \tag{6.15}$$

6.5.1 2+1 Flavour Average Momentum Model with zero asymmetry

This model is requires to requires solving $20N$ ordinary differential equations where **N** is the number comoving momentum bins being used. 9 equations for neutrinos, 9 for anti-neutrinos and two equations for Lepton asymmetry. By setting the Lepton Asymmetries L_e and L_μ and their time/temperature derivatives to zero, the system is reduced to $18N$ and the computational demand for

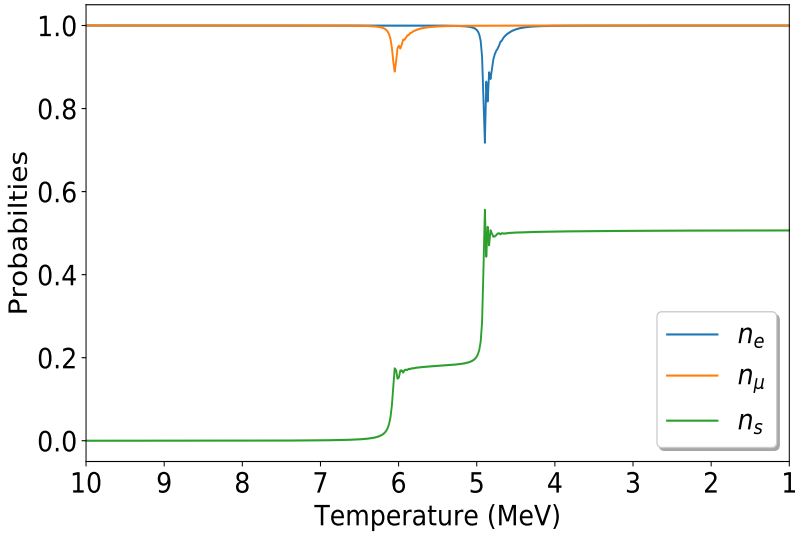

Figure 6.6: Evolution 2+1 flavour average momentum model with zero lepton asymmetry $L_e, L_\mu = 0$ with $s_{12} = 0.0112$, $s_{23} = 0.0087$ and $\delta m^2_{23} = -3 \times 10^{-3} eV$, The system was evolved from 10 MeV to 1 MeV.

performing integral over asymmetries is also removed, thus the convergence to the solution is much faster comparatively to solving a full system evolution.

The figure 6.6 shows the resonances of electron-sterile flavour system and muon-sterile flavour for negative Δm^2 in this model takes place at different temperatures indicating for inverted hierarchy and zero lepton asymmetry the active-active components are of little importance. The resonance peak for electron flavoured neutrinos appear later than muon flavour due to the additional potential of charged current that the has to be overcome by the vacuum potential, then $V_3 + \sqrt{3}V_8 = 0$, i.e. the difference between potentials felt by the electron and sterile species is zero. Similarly $-V_3 + \sqrt{3}V_8 = 0$ is the resonance condition for muon and sterile flavour neutrinos. This condition can be seen in the figure 6.7, with corresponding increase in sterile population there is a drop in absolute values for the total effective potential felt by electron neutrino $V_3 + \sqrt{3}V_8$ and muon neutrino $-V_3 + \sqrt{3}V_8$. After both the resonances there is no change in sterile population, hence the the quantity N_{eff} is locked away from evolution.

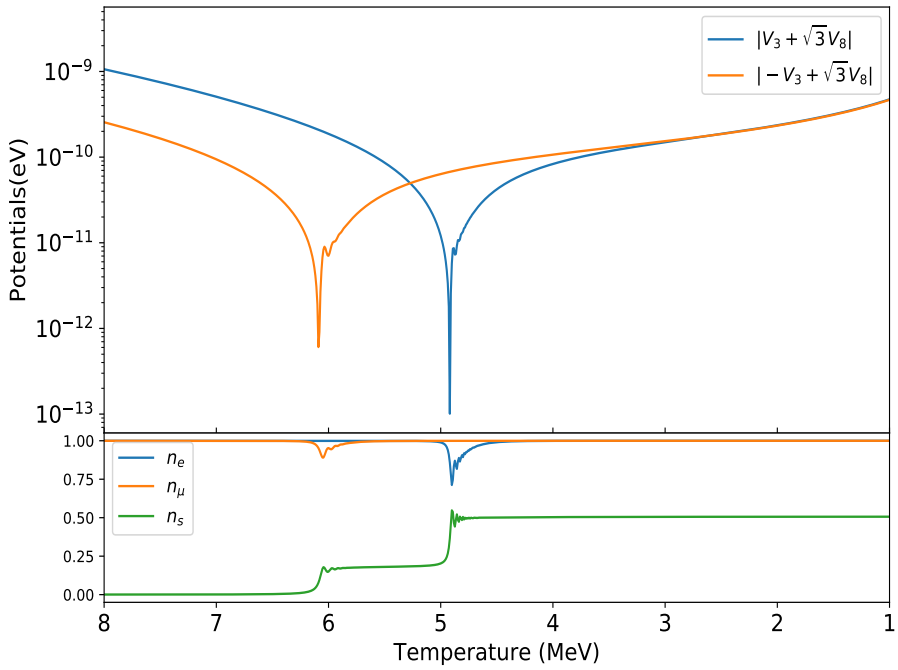

Figure 6.7: Sum of potentials for Electron flavour (blue) and Muon Flavour(orange) 2+1 flavour average momentum model with zero lepton asymmetry $L_e, L_\mu = 0$ with $s_{12} = 0.0112$, $s_{23} = 0.0087$ and $\delta m^2_{23} = -3 \times 10^{-3} eV$, The system was evolved from 10 MeV to 1 MeV.

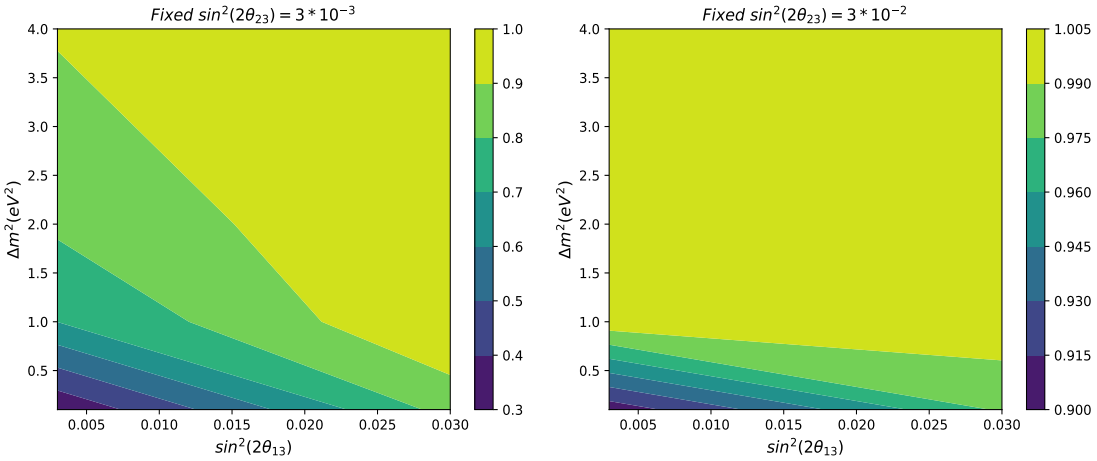

Figure 6.8: Final ΔN_{eff} for 2+1 flavour model with average momentum p = 3.15 T . The first panel $sin^2(2\theta_{23}) = 3 \times 10^{-3}$ second panel $sin^2(2\theta_{23}) = 3 \times 10^{-2}$. The system was evolved from 60 MeV to 1 MeV. The initial Lepton Asymmetry for both active flavours was taken to be 0.

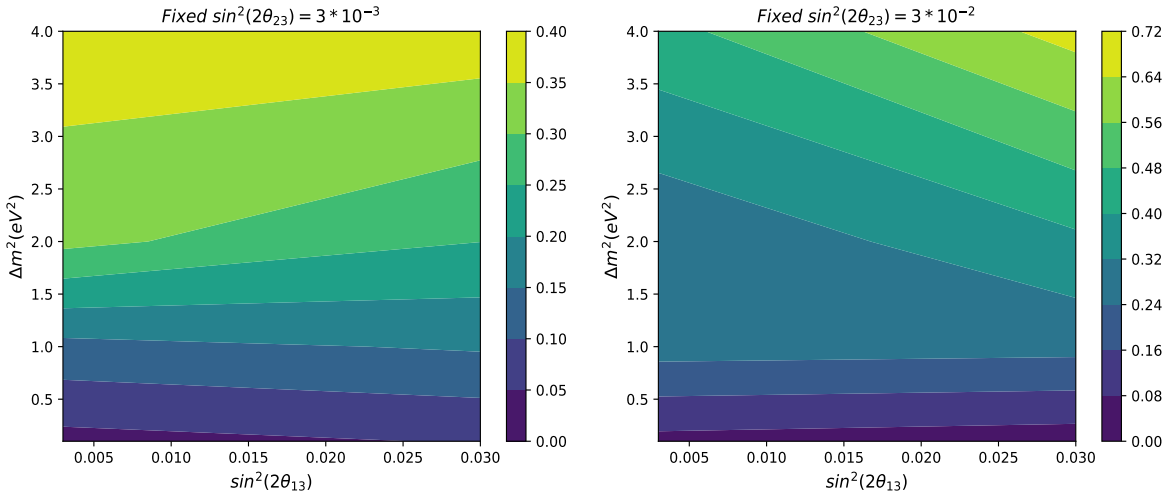

Figure 6.9: Final ΔN_{eff} for 2+1 flavour model with Average momentum p = 3.15 T. The first panel $sin^2(2\theta_{23}) = 3 \times 10^{-3}$ second panel $sin^2(2\theta_{23}) = 3 \times 10^{-2}$. The system was evolved from 60 MeV to 1 MeV. The initial Asymmetry for both active flavours was taken to be 10^{-10}.

6.5.2 2+1 Average Momentum Model with Non Zero Asymmetry

The introduction of lepton asymmetries not only shifts the ΔN_{eff} to lower values in fig. 6.9, but also shows that the asymmetries are slightly more capable of suppressing the conversion to sterile neutrinos if the electron-sterile mixing angle is larger than muon-sterile mixing angle. The features in lepton asymmetries move to higher temperatures as the mixing parameters are increased. Looking into figure 6.10 and 6.11, the major contributors for evolution of the Lepton Asymmetries are V_3 and V_8. The potential among V_3 and V_8 with the highest magnitude is specific temperature range is the driver of the evolution of the lepton asymmetries for that particular range. The closer the value of the $V^{e\mu}$ is to the main diagonal potentials is the more jittery the evolution lepton asymmetries will be. These jitter regions are the ones where the conversions to sterile neutrinos is taking place, and the active-sterile conversions is more effective when the asymmetries are low. The jitters are caused by the active-active mixing trying to compensate the empty energy states left by the conversion of active flavour to sterile neutrino.

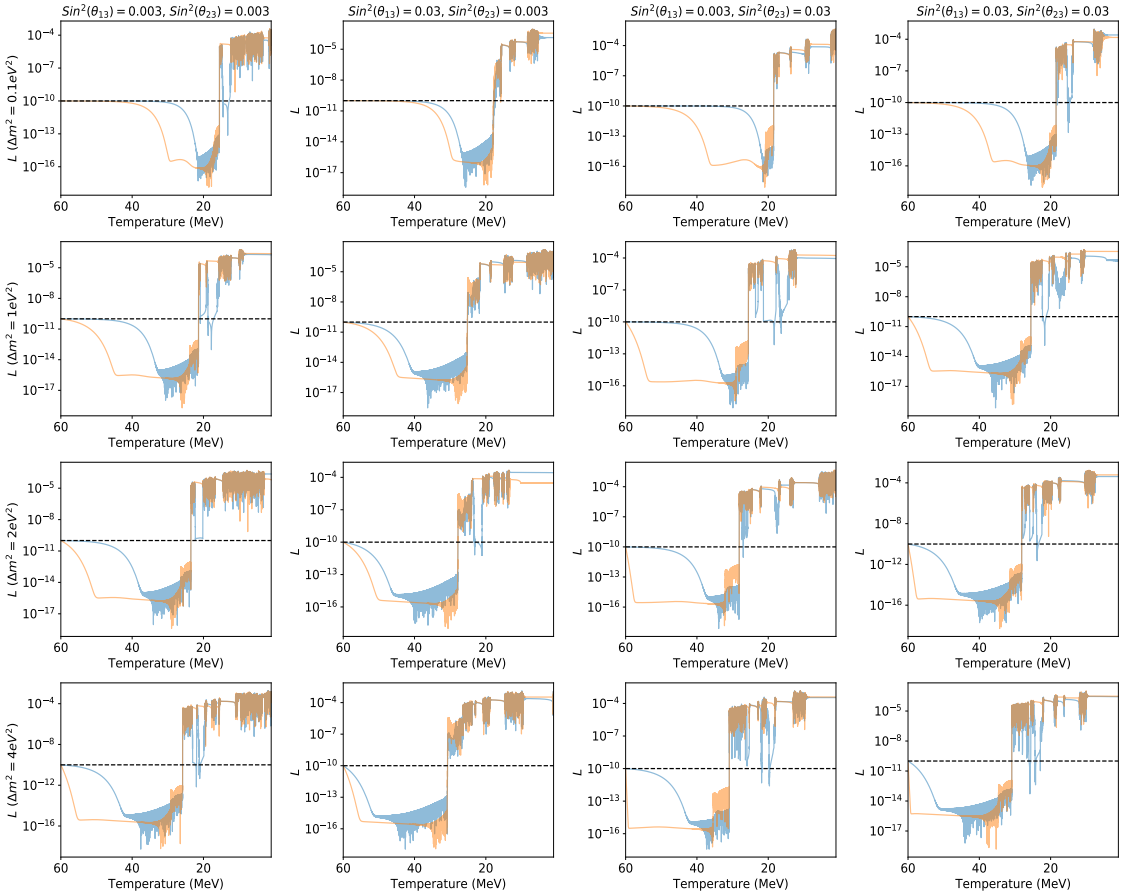

Figure 6.10: Evolution of absolute values of Lepton Asymmetries for 2+1 flavour model with Average momentum p = 3.15 T. Blue color represents the asymmetry for electron flavour and orange curve represents the lepton asymmetry for muon flavour. The first row shows evolution for $\Delta m^2 = 0.1$, second row $\Delta m^2 = 1$, third row $\Delta m^2 = 2$ and fourth row $\Delta m^2 = 4$. The system was evolved from 60 MeV to 1 MeV for different combination of $sin^2(2\theta_{13})$ and $sin^2(2\theta_{23})$ written on top. The initial Asymmetry for both active flavours was taken to be 10^{-10}.

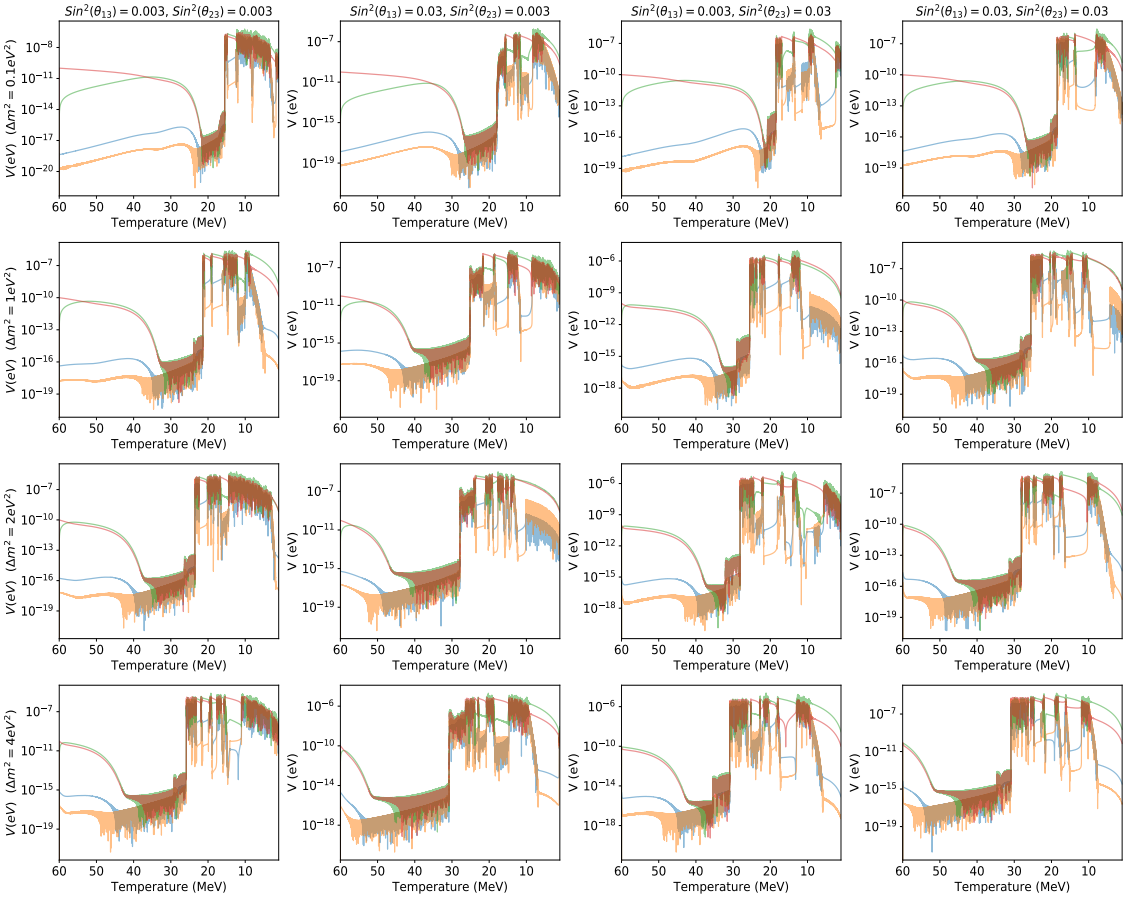

Figure 6.11: Evolution of absolute value of Potentials for 2+1 flavour model with Average momentum p = 3.15 T. Blue = $real(V^{e\mu})$, orange = $imag(V^{e\mu})$, green = V_3 and red =V_8 . The first row shows evolution for $\Delta m^2 = 0.1$, second row $\Delta m^2 = 1$, third row $\Delta m^2 = 2$ and fourth row $\Delta m^2 = 4$. The system was evolved from 60 MeV to 1 MeV for different combination of $sin^2(2\theta_{13})$ and $sin^2(2\theta_{23})$ written on top.

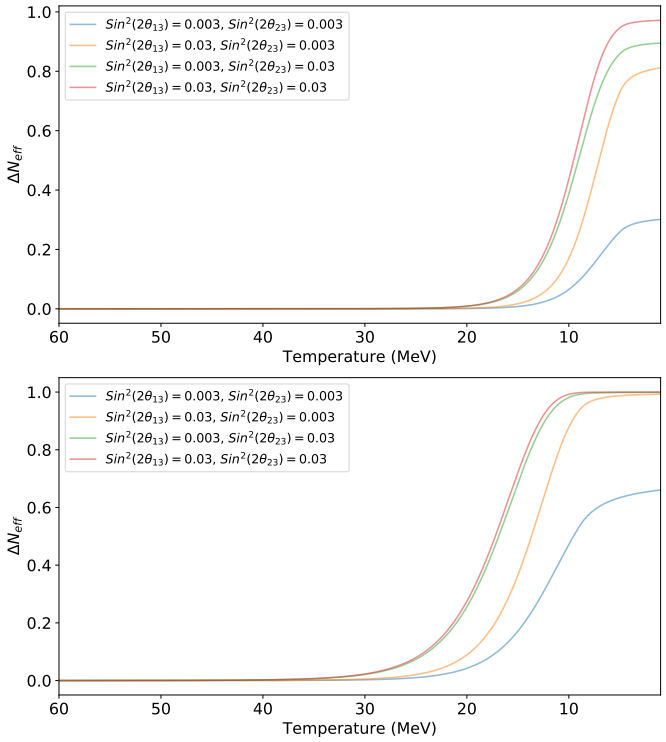

Figure 6.12: Evolution of N_{eff} for 2+1 flavour mutli-momentum model, panel one with $\Delta m^2 = 0.1eV^2$ and second panel with $\Delta m^2 = 1eV^2$. The system was evolved from 60 MeV to 1 MeV with L_e, L_μ and their time derivatives set to zero.

6.5.3 2+1 Multi-momentum Model with Zero Asymmetries

The figure 6.12 shows the curves for evolution of ΔN_{eff}. The increment in the value of ΔN_{eff} starts to takes places at low temperatures around 20 MeV for $\Delta m^2 = 0.1eV^2$ and around 30 MeV for $\Delta m^2 = 0.1eV^2$. The conversion to sterile happens for particular momentum value after it's vacuum potential crosses the medium potential of the plasma. The figure 6.13 depicts the growth of ΔN_{eff}, corresponds to normalised vacuum potentials crossing the medium potential due to plasma.

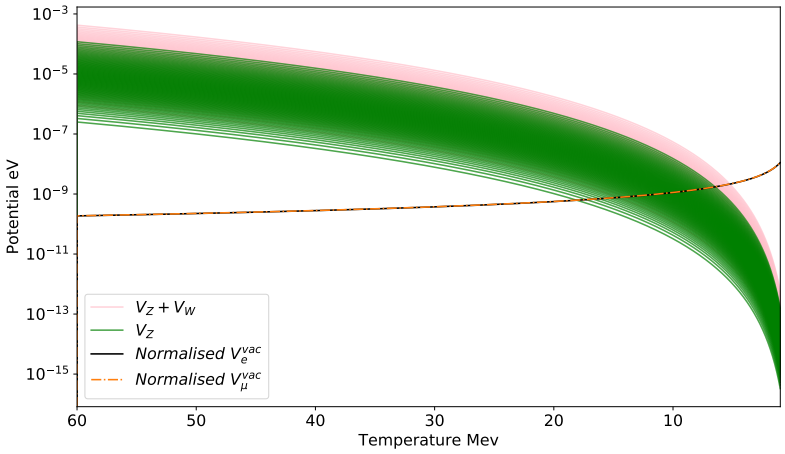

Figure 6.13: Evolution of N_{eff} for 2+1 flavour mutli-momentum model, with $\Delta m^2 = 0.1eV^2$, $sin^2(2\theta_{13}) = 0.03$ and $sin^2(2\theta_{23}) = 0.003$. The system was evolved from 60 MeV to 1 MeV with L_e, L_μ and their time derivatives set to zero.

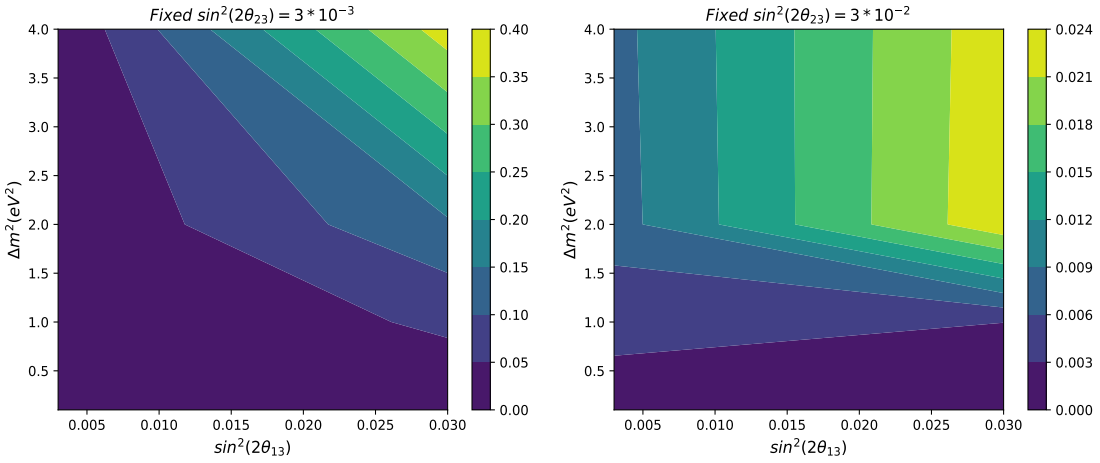

Figure 6.14: Final ΔN_{eff} for 2+1 flavour model with 100 momentum grid points. The first panel $sin^2(2\theta_{23}) = 3\times10^{-3}$ second panel $sin^2(2\theta_{23}) = 3\times10^{-2}$. The system was evolved from 60 MeV to 1 MeV. The initial Lepton Asymmetry for both active flavours was taken to be 10^{-10}.

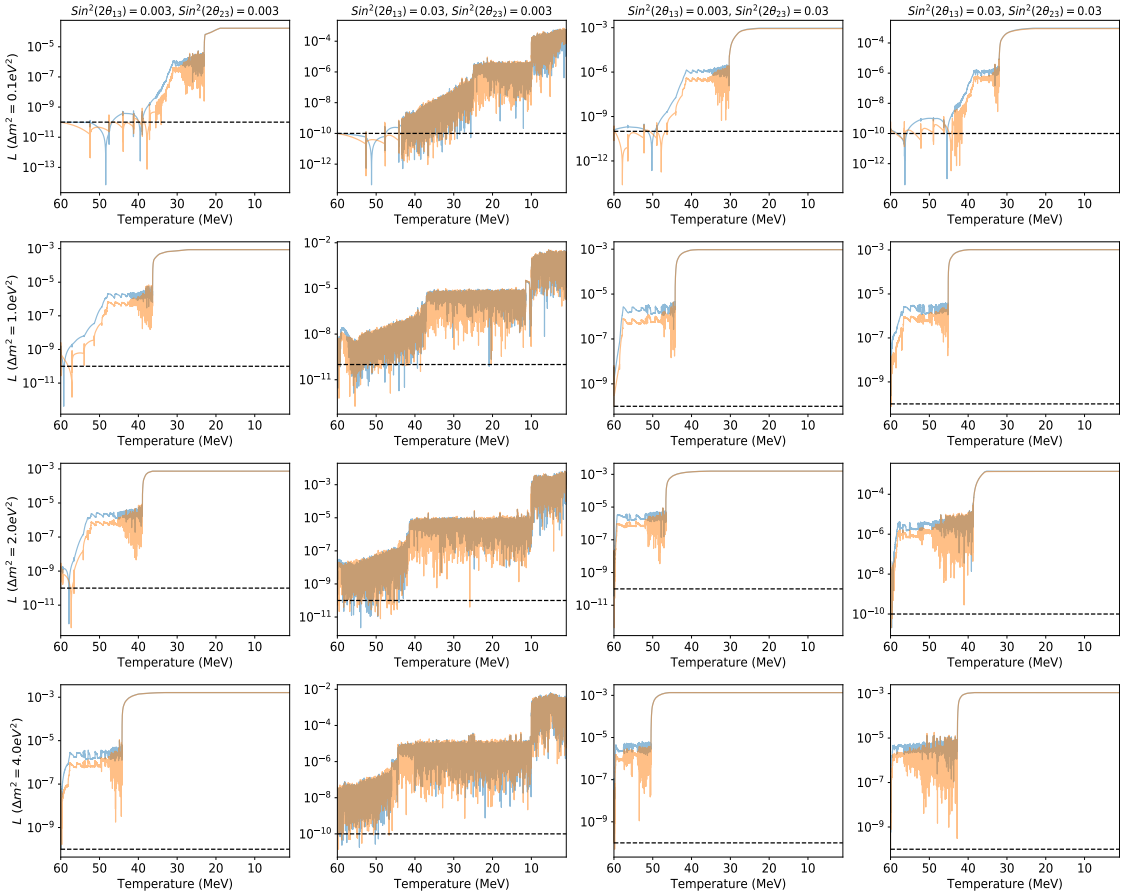

Figure 6.15: Evolution of absolute values of Lepton Asymmetries for 2+1 flavour model with 100 momentum grid points. Blue color represents the asymmetry for electron flavour and orange curve represents the lepton asymmetry for muon flavour. The first row shows evolution for $\Delta m^2 = 0.1$, second row $\Delta m^2 = 1$, third row $\Delta m^2 = 2$ and fourth row $\Delta m^2 = 4$. The system was evolved from 60 MeV to 1 MeV for different combination of $sin^2(2\theta_{13})$ and $sin^2(2\theta_{23})$ written on top. The initial Asymmetry for both active flavours was taken to be 10^{-10}.

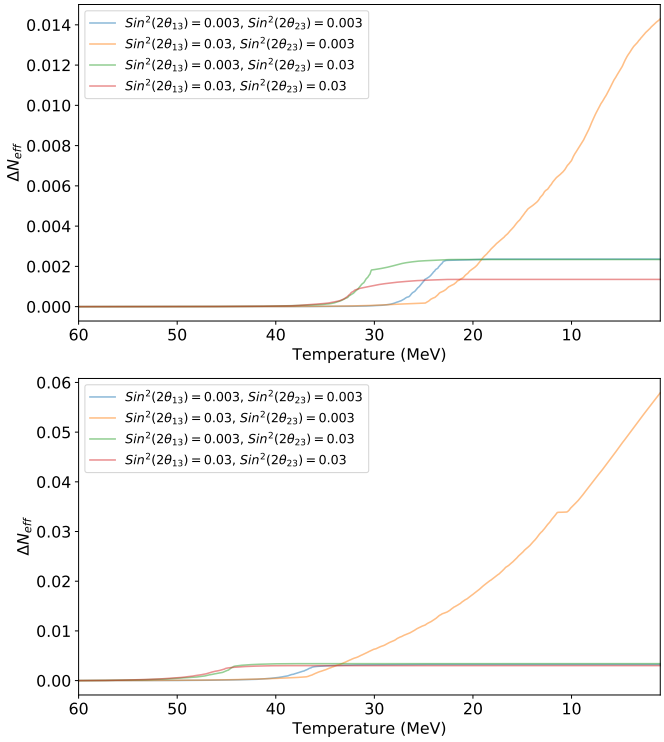

Figure 6.16: Evolution of N_{eff} for 2+1 flavour mutli-momentum model, panel one with $\Delta m^2 = 0.1eV^2$ and second panel with $\Delta m^2 = 1eV^2$. The system was evolved from 60 MeV to 1 MeV with initial of L_e, L_μ at 10^{-10}.

6.5.4 2+1 Multi-momentum Model with Non-Zero Asymmetries

The figures 6.14 and 6.15 shows a quite complicated picture of the 2+1 multi-momentum model. The figure 6.14 on one hand shows that adding non-zero initial lepton asymmetries to the system lowers the final δN_{eff} of the 2+1 system at 1 MeV. The figure 6.15 also shows amplifications for all chosen parameters ranges, and the final values of asymmetry potentials V_{L_e} and V_{L_μ} are larger than forward scattering potentials after a certain temperature, leading to a halt on sterile neutrino productions. The region of sterile neutrino is also pushed to higher temperatures as compared to zero lepton asymmetries results for 2+1 model. This means the conversion to sterile neutrinos are aided by the active-active mixing.

The pattern of increment in L_e and L_μ as seen in figure 6.15 is similar suggesting both active flavours are responsible for the growth of asymmetries. The pattern of evolution for L_e and L_μ across the range of mixing parameters scanned also show similar features in all panels of figure 6.15. It is required

for reader's understanding to name these features in the evolution, the region where asymmetries have values equal to 10^{-9} or below will be called **Plateau 1**, the region with a positive slopped increase in asymmetries to 10^{-6} or 10^{-5} levels will be called **Ramp region**, the next region after the **Ramp region** and the before the sharp vertical line increase to 10^{-3} levels will be referred to as **Plateau 2**, and the 10^{-3} increase will referred to as **Peak** and region after Peak will be called **Plateau 3**.

The mass squared difference Δm^2 and mixing angles θ_{23} and θ_{23} are not only increasing the conversion to sterile neutrinos, it's also increasing the Temperature at with the above stated features appear in lepton asymmetries leading to an earlier increase in asymmetries and blocking of conversion to sterile neutrinos. However figure 6.16 shows having mixing angle θ_{13} higher than θ_{12} delays **Peak** region of asymmetries to lower temperature leading to higher ΔN_{eff} than for other parameters in range. From figures 6.15 it's possible to see that having angle θ_{13} larger than θ_{23} makes the evolution of asymmetries more jittery due to more active-active oscillations required to fill empty electron flavour states, but the overall trend of the evolution leads to same 5 features mentioned above. To understand these feature, it is necessary to use the equations 6.14, 6.15 and track the active-active and active-sterile terms separately.

In **Plateau 1** region and **Ramp region** of figure 6.17 the terms $P_1^+ imag(V^{e\mu})$ and $P_2^- H_1$ in 6.14 and 6.15 remain larger than other active-active term $P_2^+ real(V^{e\mu})$ and these first two terms summed up are larger than $P_7^- V_6$ and smaller than $P_5^- V_4$. This means the active-active oscillation carry over the changes from electron-sterile flavour mixing to muon-sterile mixing. The first and the last terms of the equations 6.14 and 6.15 are keeping the values of the derivatives dP_e^- and dP_μ^- from changing much, the increase in Lepton Asymmetries in **Ramp region** of electron-sterile sector is caused by the term $P_2^- H_1$ increasing with temperature and then carried over to muon-sterile sector. The **Ramp region** finally stops with the third active-active term $P_2^+ real(V^{e\mu})$ becomes comparable to first 2 active-active terms. The **Plateau 2** is the region where the conversion to sterile neutrino as well as active-active are maximum. This results in increase in ΔN_{eff} at higher temperatures as compared to 1+1 model. The figure 6.18 shows the ΔN_{eff} slope of changes suddenly at the **Peak** in L_e and L_μ indicating the lepton asymmetries potentials have

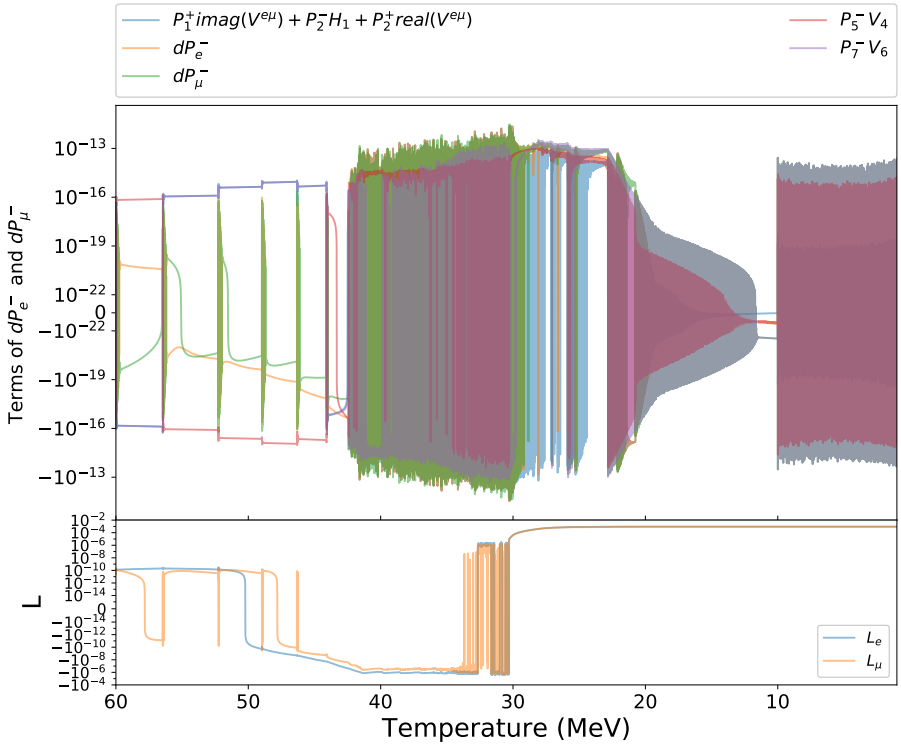

Figure 6.17: The top panel show the evolution of terms in dP_e^- and dP_μ^- for 2+1 flavour mutli-momentum model with $\Delta m^2 = 0.1eV^2$, $sin^2(2\theta_{23}) = 3 \times 10^{-3}$ and $sin^2(2\theta_{23}) = 3 \times 10^{-2}$, and second panel shows the Lepton asymmetries for both active flavours. The system was evolved from 60 MeV to 1 MeV with initial of L_e, L_μ at 10^{-10}. The legend for first panel is on the top, the blue curve is for initial region is under the violet curve.

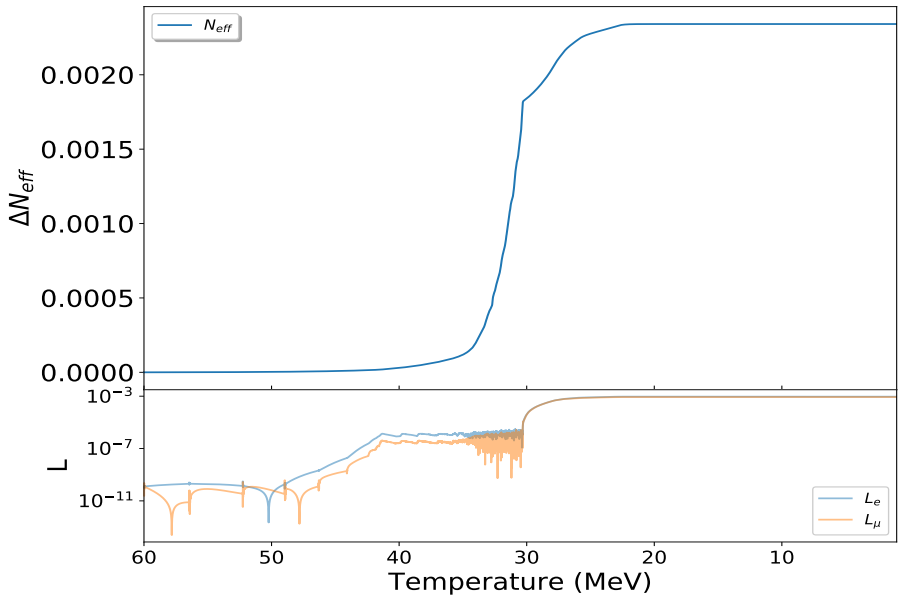

Figure 6.18: The top panel show the evolution of ΔN_{eff} for 2+1 flavour mutli-momentum model with $\Delta m^2 = 0.1eV^2$, $sin^2(2\theta_{23}) = 3 \times 10^{-3}$ and $sin^2(2\theta_{23}) = 3 \times 10^{-2}$, and second panel shows the absolute values of Lepton asymmetries for both active flavours. The system was evolved from 60 MeV to 1 MeV with initial of L_e, L_μ at 10^{-10}.

started dominating and the conversion to sterile are shut off by after the entire momentum grid have V_{L_e} and V_{L_μ} larger than charged and neutral current potentials in **Plateau 3**.

The **Peak** in Lepton Asymmetries is due resonances occurring for small values for comoving momentum x. In figure 6.19 the active-sterile resonances occur for both anti-neutrino active flavours, since there is loss of active flavours from anti-matter populations the L_e and L_μ will move towards positive values or matter side, thus the chemical potentials would allow more refilling of matter states than anti-matter states, thereby causing the anti-matter empty states to remain unfilled for longer. In the **Plateau 3** region the values for dP_e^- and dP_μ^- remain relatively smaller than L_e and L_μ to cause any significant change in them, thereby the values for Lepton Asymmetries remain stable for rest of the temperature range. The figure 6.17 fails to capture this increase in asymmetry as it only occurs for a few small comoving momentum points and it gets overwhelmed by the normalised values from the spectrum.

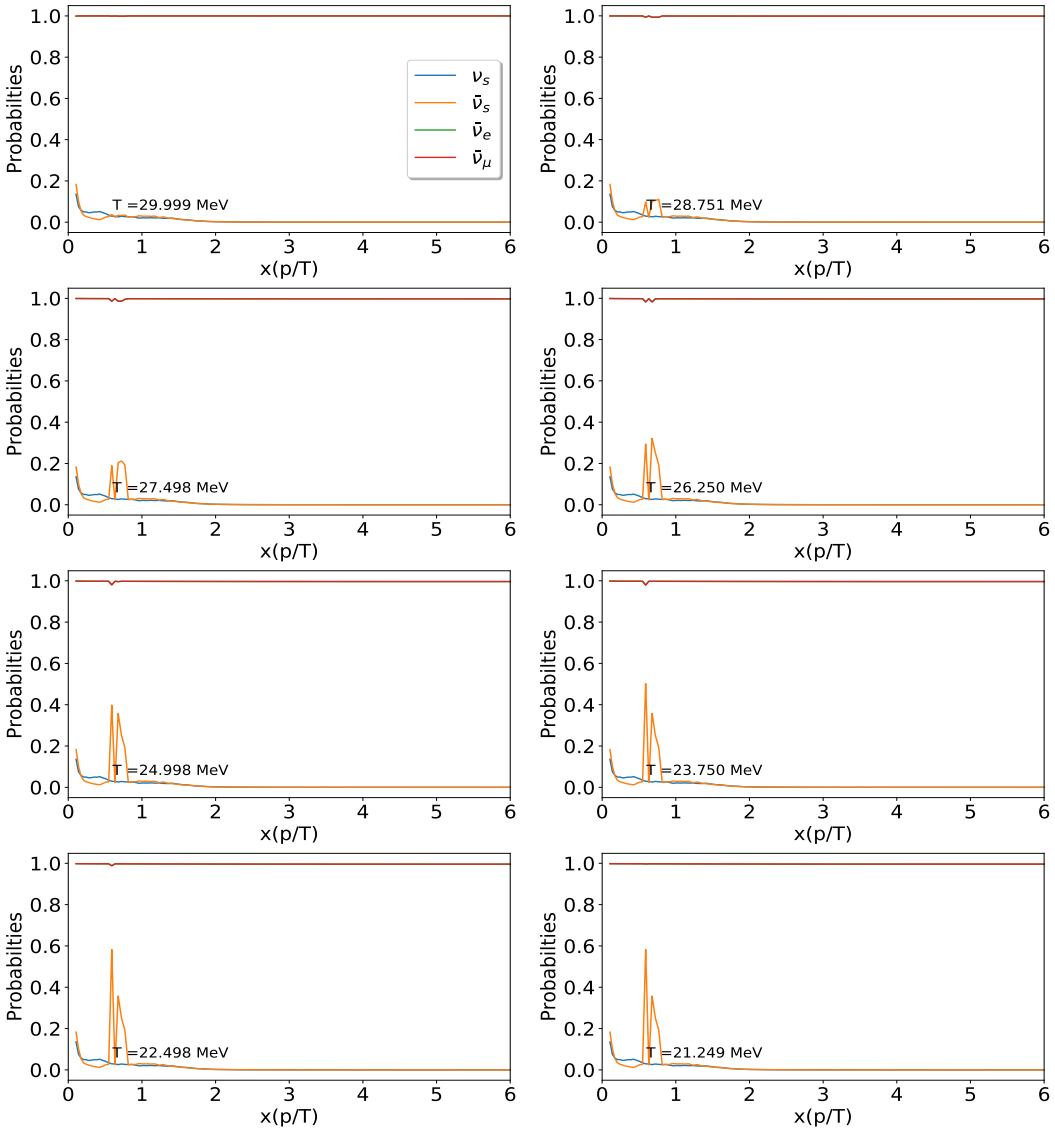

Figure 6.19: The evolution of active-sterile resonances at small comoving momentum **x** for 2+1 flavour mutli-momentum model with $\Delta m^2 = 0.1eV^2$, $sin^2(2\theta_{23}) = 3 \times 10^{-3}$ and $sin^2(2\theta_{23}) = 3 \times 10^{-2}$ for temperature 30 The system was evolved from 60 MeV to 1 MeV with initial of L_e, L_μ at 10^{-10}.

7 Discussion

7.1 Summary of findings

The result from 2+1 Average momentum model and 2+1 Multi-momentum model with non-zero initial asymmetries display increase in L_e and L_μ asymmetries to orders of 10^{-4} and 10^{-3}, that slows the production of sterile neutrino and stops them becoming fully thermalised. The 2+1 multi-momentum model shows a larger suppression on the final values of ΔN_{eff} than average momentum model.

7.1.1 Average momentum 2+1 model

The value of ΔN_{eff} from the figure 6.9 suggests that the value for Δm^2 above $3\ eV^2$ are the Planck 2018's limit of $2.96^{+0.34}_{-0.33}$. The range between 3×10^{-3} and 3×10^{-2} is suitable for $Sin^2(2\theta_{13})$ with Δm^2 below $3\ eV^2$ and $Sin^2(2\theta_{23}) = 3 \times 10^{-3}$.

But high value for $sin^2(2\theta_{23})$ restricts the choice to for below Δm^2 in sub $2\ eV^2$ range and higher mixing angles for electron and sterile flavour become less possible.

This model is however doesn't cut off the sterile productions completely even at low temperatures, the jitters in lepton asymmetries indicate the sterile neutrino the value for asymmetries of orders 10^{-4} are insufficient to fully halt the sterile neutrino production for the range of mixing parameters.

7.1.2 Multi-momentum 2+1 model

The multi-momentum model shows more complicated behaviour but consistent behaviour as compared to average momentum model. The absolute values for Lepton Asymmetries do not drop to lower magnitudes and stay stably at same order or get amplified with decreasing temperature. The conversion to sterile flavour is mostly occurs at low comoving momentum values, and the conversion to sterile neutrinos stop when the Lepton Asymmetries reach a magnitude of 10^{-3}.

The suppression of final value of ΔN_{eff} is large when θ_{23} is taken to be 0.03 and the whole parameter space becomes sub 0.1 ΔN_{eff} level which is well within Planck 2018's allowed range. However when $\theta_{23} = 0.003$ the system gives higher ΔN_{eff} only a few points with high mass squared values are excluded.

When the mixing angle θ_{13} is set higher than θ_{23}, the system shows more production of sterile neutrino as the temperature at which the **Peak** occurs is lower to around 10 MeV, thereby increasing the ΔN_{eff} as compared other combination of angles.

8 Perspectives

The have been a similar 2+1 multi-momentum study done in [23], however they have collision terms that conserve Lepton Number, they fix the Lepton Asymmetry amplitude to 10^{-2} and 10^{-3} levels and their momentum grid had only 21 points. The study presented in this thesis has more momentum resolution than it and has 2 dynamic asymmetries, thus it's an improvement over their study. Another study of 3+1 model has been done in the paper [24] with $\Delta m^2 = 1\ eV^2$ between first and fourth mass eigenstates. They find with no lepton symmetry even with low mixing the sterile neutrino can be thermalised leading to $N_{eff} = 4$.

There would be an upcoming paper continuing from this thesis, that would elaborate more on the features found in multi-momentum 2+1 model and would include cases where the initial lepton asymmetries would be taken to be unequal.

Lastly, the code for the simulation should be run at higher temperature resolutions and lower tolerance for differential equation solvers. The program being computational intensive raises the solver time and the required runs would take much longer than the allowed time limit of the supercomputer cluster available. The basic program written in python which was greatly limited by the speed of the language. Several workarounds and optimisations were made to make the overall computation time lower and achieving solver convergence, these include figuring out the constants for each run prior to solving of the **20N** differential equation, reducing number of very small and very large power multiplications, pre-calculation of predictable evolution variables. These modification and optimisations of the code can be carried over to different programming languages.

The speed requirements could be reduced by writing the program in a faster computer language such as C++, which would require less optimizations than python to run for higher resolution runs for both the comoving mo-

mentum and the temperature. Using a GPU programming language CUDA could be leveraged for parallel computation of the momentum grid simultaneously and increasing the scaling capacity of the algorithm. The use of modern CPU(s)/GPU(s) with built-in matrix multiplication hardware could bring a lot of freedom to the simulation limits that is imposed by the hardware capacities.

Bibliography

9

[1] S. P. Mikheyev and A. Yu. Smirnov. „Resonance enhancement of oscillations in matter and solar neutrino spectroscopy“. In: *Yadernaya Fizika* 42 (Jan. 1985), pp. 1441–1448.

[2] Q. R. Ahmad, R. C. Allen, T. C. Andersen, *et al.* „Direct Evidence for Neutrino Flavor Transformation from Neutral-Current Interactions in the Sudbury Neutrino Observatory“. In: *Phys. Rev. Lett.* 89 (1 June 2002), p. 011301. DOI: 10.1103/PhysRevLett.89.011301. URL: https://link.aps.org/doi/10.1103/PhysRevLett.89.011301.

[3] D Décamp, B Deschizeaux, J P Lees, *et al.* „Determination of the number of light neutrino species“. In: *Phys. Lett. B* 231.CERN-EP-89-132 (Oct. 1989), 519–529. 20 p. DOI: 10.1016/0370-2693(89)90704-1. URL: http://cds.cern.ch/record/201511.

[4] L. M. Carpenter and A. Rajaraman. „Revisiting constraints on fourth generation neutrino masses“. In: *Physical Review D* 82.11 (Dec. 2010). ISSN: 1550-2368. DOI: 10.1103/physrevd.82.114019. URL: http://dx.doi.org/10.1103/PhysRevD.82.114019.

[5] Gianpiero Mangano, Gennaro Miele, Sergio Pastor, *et al.* „Relic neutrino decoupling including flavour oscillations“. In: *Nuclear Physics B* 729.1-2 (Nov. 2005), pp. 221–234. ISSN: 0550-3213. DOI: 10.1016/j.nuclphysb.2005.09.041. URL: http://dx.doi.org/10.1016/j.nuclphysb.2005.09.041.

[6] A. Aguilar-Arevalo *et al.* „Evidence for neutrino oscillations from the observation of $\bar{\nu}_e$ appearance in a $\bar{\nu}_\mu$ beam“. In: *Phys. Rev. D* 64 (2001), p. 112007. DOI: 10.1103/PhysRevD.64.112007. arXiv: hep-ex/0104049.

[7] A. A. Aguilar-Arevalo, C. E. Anderson, S. J. Brice, *et al.* „Event Excess in the MiniBooNE Search forŕŕeOscillations“. In: *Physical Review Letters* 105.18 (Oct. 2010). ISSN: 1079-7114. DOI: 10.1103/physrevlett.

105.181801. URL: http://dx.doi.org/10.1103/PhysRevLett.105.181801.

[8] G. Mention, M. Fechner, Th. Lasserre, *et al.* „Reactor antineutrino anomaly“. In: *Physical Review D* 83.7 (Apr. 2011). ISSN: 1550-2368. DOI: 10.1103/physrevd.83.073006. URL: http://dx.doi.org/10.1103/PhysRevD.83.073006.

[9] N. Aghanim, Y. Akrami, M. Ashdown, *et al.* „Planck 2018 results“. In: *Astronomy Astrophysics* 641 (Sept. 2020), A6. ISSN: 1432-0746. DOI: 10.1051/0004-6361/201833910. URL: http://dx.doi.org/10.1051/0004-6361/201833910.

[10] Sacha Davidson, Enrico Nardi, and Yosef Nir. „Leptogenesis“. In: 466.4-5 (Sept. 2008), pp. 105–177. DOI: 10.1016/j.physrep.2008.06.002. arXiv: 0802.2962 [hep-ph].

[11] M. H. Ahn, S. Aoki, H. Bhang, *et al.* „Indications of Neutrino Oscillation in a 250ăkm Long-Baseline Experiment“. In: *Physical Review Letters* 90.4 (Jan. 2003). ISSN: 1079-7114. DOI: 10.1103/physrevlett.90.041801. URL: http://dx.doi.org/10.1103/PhysRevLett.90.041801.

[12] K. Eguchi, S. Enomoto, K. Furuno, *et al.* „First Results from KamLAND: Evidence for Reactor Antineutrino Disappearance“. In: *Physical Review Letters* 90.2 (Jan. 2003). ISSN: 1079-7114. DOI: 10.1103/physrevlett.90.021802. URL: http://dx.doi.org/10.1103/PhysRevLett.90.021802.

[13] Steen Hannestad, Irene Tamborra, and Thomas Tram. „Thermalisation of light sterile neutrinos in the early universe“. In: *JCAP* 07 (2012), p. 025. DOI: 10.1088/1475-7516/2012/07/025. arXiv: 1204.5861 [astro-ph.CO].

[14] S.P. Mikheev and A.Yu. Smirnov. „Resonant amplification of neutrino oscillations in matter and solar neutrino spectroscopy“. In: *Nuovo Cim. C* 9 (1986), pp. 17–26. DOI: 10.1007/BF02508049.

[15] Dirk Notzold and Georg Raffelt. „Neutrino Dispersion at Finite Temperature and Density“. In: *Nucl. Phys. B* 307 (1988), pp. 924–936. DOI: 10.1016/0550-3213(88)90113-7.

[16] K Enqvist, K Kainulainen, and J Maalampi. „Refraction and oscillations of neutrinos in the early universe“. In: *Nuclear Physics B* 349.3 (1991), pp. 754–790. ISSN: 0550-3213. DOI: https://doi.org/10.1016/0550-3213(91)90397-G. URL: http://www.sciencedirect.com/science/article/pii/055032139190397G.

[17] Bruce H.J. McKellar and Mark J. Thomson. „Oscillating doublet neutrinos in the early universe“. In: *Phys. Rev. D* 49 (1994), pp. 2710–2728. DOI: 10.1103/PhysRevD.49.2710.

[18] M. A. Rudzskii. „Kinetic equations for neutrino spin- and type-oscillations in a medium“. In: 165.1 (Mar. 1990), pp. 65–81. DOI: 10.1007/BF00653658.

[19] Nicole F. Bell, Raymond R. Volkas, and Yvonne Y. Y. Wong. „Relic neutrino asymmetry evolution from first principles“. In: *Physical Review D* 59.11 (Apr. 1999). ISSN: 1089-4918. DOI: 10.1103/physrevd.59.113001. URL: http://dx.doi.org/10.1103/PhysRevD.59.113001.

[20] Bruce H. J. McKellar and Mark J. Thomson. „Oscillating neutrinos in the early Universe“. In: *Phys. Rev. D* 49 (6 Mar. 1994), pp. 2710–2728. DOI: 10.1103/PhysRevD.49.2710. URL: https://link.aps.org/doi/10.1103/PhysRevD.49.2710.

[21] G. Sigl and G. Raffelt. „General kinetic description of relativistic mixed neutrinos“. In: *Nuclear Physics B* 406.1 (1993), pp. 423–451. ISSN: 0550-3213. DOI: https://doi.org/10.1016/0550-3213(93)90175-O. URL: http://www.sciencedirect.com/science/article/pii/055032139390175O.

[22] Kimmo Kainulainen and Antti Sorri. „Oscillation induced neutrino asymmetry growth in the early universe“. In: *Journal of High Energy Physics* 2002.02 (Feb. 2002), pp. 020–020. DOI: 10.1088/1126-6708/2002/02/020. URL: https://doi.org/10.1088%2F1126-6708%2F2002%2F02%2F020.

[23] Ninetta Saviano, Alessandro Mirizzi, Ofelia Pisanti, *et al.* „Multimomentum and multiflavor active-sterile neutrino oscillations in the early universe: Role of neutrino asymmetries and effects on nucleosynthesis“. In: *Physical Review D* 87.7 (Apr. 2013). ISSN: 1550-2368. DOI: 10.1103/physrevd.87.073006. URL: http://dx.doi.org/10.1103/PhysRevD.87.073006.

[24] Sergio Pastor. „Active-sterile neutrino oscillations in the early Universe with the complete mixing matrix“. In: *Journal of Physics: Conference Series* 1468 (Feb. 2020), p. 012005. DOI: 10.1088/1742-6596/1468/1/012005. URL: https://doi.org/10.1088%2F1742-6596%2F1468%2F1%2F012005.